Catalytic Synthesis of Carbon Nanotubes and Nanofibers

Kenneth B. K. Teo

Department of Engineering, University of Cambridge, Cambridge CB2 1PZ, United Kingdom

Charanjeet Singh

Department of Materials Science and Metallurgy, University of Cambridge, Cambridge CB2 3QZ, United Kingdom

Manish Chhowalla, William I. Milne

Department of Engineering, University of Cambridge, Cambridge CB2 1PZ, United Kingdom

CONTENTS

1. INTRODUCTION

Carbon nanotubes and nanofibers are graphitic filaments/whiskers with diameters ranging from 0.4 to 500 nm and lengths in the range of several micrometers to millimeters. Carbon nanofibers and nanotubes are grown by the diffusion of carbon (via catalytic decomposition of carbon containing gases or vaporized carbon from arc discharge or laser ablation) through a metal catalyst and its subsequent precipitation as graphitic filaments [1–6]. Three distinct structural types of filaments have been identified based on the angle of the graphene layers with respect to the filament axis [5, 7], namely *stacked*, *herringbone* (or *cup-stacked* [8]), and *nanotubular* [9] as shown in Figure 1.

It can be seen that the graphite platelets are perpendicular to the fiber axis in the stacked form, the graphene platelets are at an angle to the fiber axis in the herringbone form, and tubular graphene walls are parallel to the fiber axis in the nanotube. In the literature today, the common practice is to classify the stacked and herringbone forms of graphitic filaments under the general nomenclature of "nanofibers" whereas "nanotube" is used to describe the case where tubular graphene walls are parallel to the filament axis. Other definitions used today are that highly crystallized tubular structures are nanotubes whereas defective ones are nanofibers, or tubular structures ~20 nm or below in diameter are nanotubes but larger diameter filaments are fibers. In this work, we prefer to use the term nanotube to describe carbon filaments with tubular graphene walls parallel to the axis and use the term nanofiber for carbon filaments with graphene layers at other angles. This is because special physical properties arise from the "nanotube" structure which distinguish it from the "nanofiber" structure, which itself has other advantageous properties, as will be described later.

Carbon nanofibers and nanotubes have been synthesized since the 1960s, but why has one particular form (i.e. the nanotube) received so much attention recently? In 1991, Iijima reported that highly graphitized carbon nanotubes, formed from the arc discharge of graphite electrodes, contained several coaxial tubes and a hollow core [9]. This important discovery led to the realization that with graphene tubes parallel to the filament axis, these highly crystallized tubular carbon structures would inherit several important properties of "intraplane" graphite. In particular, a nanotube exhibits high electrical conductivity, thermal conductivity, and mechanical strength along its axis. As there are very few open edges and dangling bonds in the structure, nanotubes are also very inert and species tend

ISBN: 1-58883-001-2/$35.00

Encyclopedia of Nanoscience and Nanotechnology
Edited by H. S. Nalwa
Volume X: Pages (1–22)

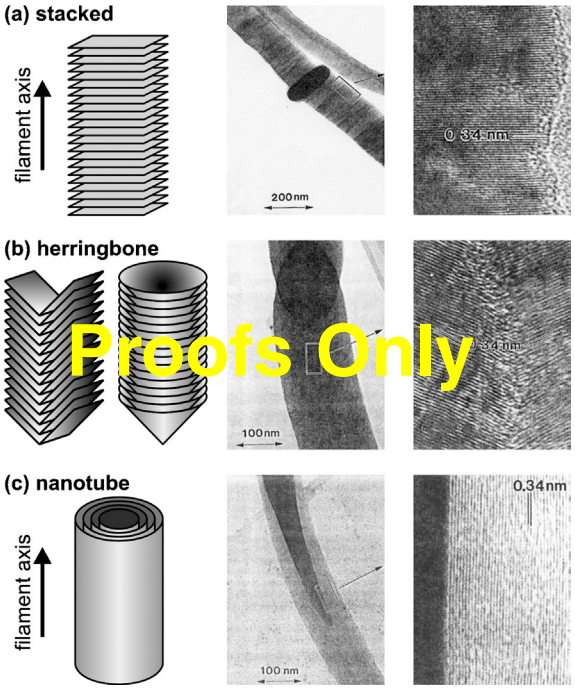

Figure 1. The three structural forms of carbon nanofibers, classified by the angle of the graphene layers/platelets with respect to the filament axis. Adapted with permission from [5], N. M. Rodriguez et al., *Langmuir* 11, 3862 (1995). © 1995, American Chemical Society.

to be physically adsorbed onto graphene walls rather than chemically react with them. Note that carbon nanotubes are completely covalently bonded which implies that as electrical conductors, they would not suffer from electromigration or atomic diffusion like metals. These properties make carbon nanotubes a technologically important material for various electronic and mechanical applications as will be listed later. The stacked and herringbone nanofibers tend to be investigated solely for energy storage applications such as electrodes for lithium batteries or fuel cells as small ions/molecules can enter via open edges and intercalate between the graphene layers. Already, large amounts of nanofibers can be purchased commercially from companies such as Hyperion Catalysis International, Applied Sciences Incorporated, Catalytic Materials, Showa Denko, and Nanomirae [10]. Nanotubes are also available commercially from companies such as Carbon Nanotechnologies Inc., Iljin Nanotech, and NanoLab among many others listed in [11].

Nanotubes are further classified into two types, namely multiwall and single wall [9, 12, 13]. The multiwall carbon nanotube contains several concentric, coaxial graphene cylinders with interlayer spacings of ~0.34 nm [14]. Note that this spacing is larger than single crystal graphite (0.335 nm). Recent studies have shown that the intershell spacing can actually range from 0.34 to 0.39 nm, where the intershell spacing decreases with increasing carbon nanotube diameter, and this effect is more pronounced in small diameter nanotubes (<15 nm) due to the high curvature [15, 16]. The geometrical constraints in forming the seamless "honeycomb" graphene cylinders cause the layers to be uncorrelated with respect to one another, which is in contrast to crystalline graphite that exhibits perfect "ABAB" layer stacking [17]. Thus, multiwall carbon nanotubes tend to exhibit the properties of turbostratic graphite whose layers are essentially uncorrelated. For example, in highly crystallized multiwall carbon nanotubes (such as those obtained by arc discharge), it has been shown that if contacted on the outside, the electric current is conducted through its outermost shell only [18].

In the case of single wall carbon nanotubes, the structure consists of a single graphene cylinder and special properties emerge from the strong one-dimensionality and crystalline perfection of the structure. Single wall carbon nanotubes can be metallic (0 eV bandgap) or semiconducting (typically 0.4–0.7 eV bandgap) depending on the geometrical characteristics of their structure, namely the orientation of the hexagons with respect to the nanotube axis (i.e., chirality) and inversely proportional to the diameter [19–21]. Reviews on the electronic properties of carbon nanotubes are presented in [22–24]. In the case of a multiwall carbon nanotube where conduction occurs through the outermost shell, the large diameter of the outer nanotube causes the gap to approach 0 eV and the nanotube is essentially nonsemiconducting. Table 1 lists several reported properties of carbon nanotubes.

Table 1. Properties of carbon nanotubes; see also [34].

Mechanical properties		Thermal properties at room temperature	
Young's modulus of multiwall nanotubes	~1–1.2 TPa [25, 26]	Thermal conductivity of single wall nanotube	1750–5800 W mK [28]
Young's modulus of single wall nanotube ropes	~1 TPa [27]	Thermal conductivity of multiwall nanotube	>3000 W mK [29]
Tensile strength of single wall nanotube ropes	~60 GPa [25]		
Electrical properties		**Electronic properties**	
Typical resistivity of single and multiwall nanotube	10^{-6} Ω m [22, 30]	Single wall nanotube bandgap—whose n–m is divisible by 3	0 eV [22] (metallic)
Typical maximum current density	10^{7}–10^{9} A cm^2 [31, 32]	whose n–m is nondivisible by 3	0.4–0.7 eV [20, 21] (semiconducting)
Quantized conductance, theoretical/measured	$(6.5\ \text{k}\Omega)^{-1}/(12.9\ \text{k}\Omega)^{-1}$ [22, 33]	Multiwall nanotube bandgap	~0 eV [22] (nonsemiconducting)

Carbon nanotubes and nanofibers are being investigated for a wide range of applications today. Reviews of carbon nanotube applications are presented in [24, 35–42], and only an overview is presented in this chapter. Let us first consider the nanotube as a high aspect ratio, electrically conductive wire with diameter in the nanometer range. These structures are highly desirable as field emission tips for applications such as field emission displays [43–48], X-ray tubes [49], electron sources for microscopy and lithography [50], gas discharge tubes [51], and vacuum microwave amplifiers. The use of nanotubes as a field emission electron source has recently been commercialized in a portable X-ray source by Oxford Instruments [52]. Nanofibers have also been investigated as electron sources [53, 54]. The high aspect ratio and small diameter of the nanotube is also desirable for scanning probe tips [55–57]. In fact, nanotube-based scanning probe tips ("Probemax") are commercially available today from nPoint (also known as Piezomax) [58].

Single wall carbon nanotubes, which can be electronically semiconducting, are also being investigated as transistors or logic elements [59–62]. Containing only one carbon tube, the electronic properties of the carbon nanotubes are highly sensitive to adsorbed molecules/species [63, 64]. Although this implies that in logic circuits, the nanotubes must be suitably encapsulated, the high sensitivity of the nanotubes can be advantageously utilized in chemical or biological sensors to detect poisonous or dangerous gases in the environment. In addition, the coherent nature of electron transport in well-crystallized nanotubes would find these structures applicable in spin–electronic devices [65]. Carbon nanotubes could also be used as electromechanical sensors as their electrical characteristics respond to mechanical deformation of their structure [66].

Another interesting application for these structures is as electrodes in electrochemical supercapacitors [35, 67–71]. When nanotubes/fibers are produced enmasse (i.e., woollike or forestlike), they have large surface areas which could lead to higher charge storage capabilities than standard capacitors and batteries [35, 72]. The cycle characteristics of lead acid and lithium ion batteries can also be improved when carbon nanofibers are used as fillers in the battery electrodes [73]. The high electrical conductivity and relative inertness of nanotubes make them potential candidates as electrodes in electrochemical reactions too [74, 75]. The large surface area of nanotubes, both inside and outside, can be usefully employed to support reactant particles in catalytic conversion reactions [76, 77]. It was also proposed that hydrogen could also be stored among and inside nanotubes/nanofibers for fuel cell applications [7, 76–81], although recent results show that the amount of hydrogen stored is not as high as originally anticipated [82]. Nanotubes can also mechanically deflect under electric stimulation (e.g., due to charge induced on the nanotubes) and this opens up applications such as cantilevers or actuators [35, 83–85]. The use of nanotubes and nanofibers as filters or membranes for molecular transport has been recently proposed [86].

The exceptional mechanical properties and low weight of nanotubes and nanofibers make them potential filling materials in polymer composites. Nanotubes and nanofibers can improve the strength and stiffness of a polymer, as well as add multifunctionality (such as electrical conductivity) to polymer based composite systems [87–95]. Carbon nanotubes should be ideal reinforcing fibers for composites due to their high aspect ratio and high in-axis strength [96]. Furthermore, carbon nanotubes, unlike macroscopic carbon fibers, are short enough to flow through conventional polymer processing equipment so that complicated shapes or small parts could be molded from their composites [96, 97]. As fillers for composites, single wall carbon nanotubes are preferred to multiwall nanotubes because the inner layers of the multiwall nanotubes contribute little under structural loading and thus would reduce the stiffness for a given volume fraction of tubes [26, 96].

It is evident that for the various different applications, nanotubes or nanofibers of different morphologies are required. For instance, scanning probe applications require a single high aspect ratio nanotube whereas polymer strengthening requires "masses" of nanotubes/nanofibers. Field emission applications ideally require vertically aligned nanotubes which are spaced about twice their height apart [98–100], whereas horizontally aligned nanotubes are more suited for electrical transport or electronic (transistor/spin) applications. The great flexibility of catalytic chemical vapor deposition (CVD) is that this technique can be adapted to producing nanotubes and nanofibers for *virtually all* these applications.

In the case of nanotubes, chemical vapor deposition is very different from the other two common methods used for nanotube production, namely arc discharge [101, 102] and laser ablation [30]. Arc discharge and laser ablation can be classified as high temperature (>3000 K) and short time reactions (μs–ms), whereas catalytic chemical vapor deposition is a medium temperature (700–1400 K) and long time reaction (typically minutes to hours). Although carbon filament/nanofiber growth by catalytic chemical vapor deposition was established in the 1960s–1980s [3, 4, 103–105], much of the fundamental work on the properties of nanotubes in the early 1990s was performed on nanotubes produced by arc discharge and laser ablation because of their superior straightness and crystallinity due to the high temperature deposition. The main technological drawbacks with arc discharge and laser ablation were that the nanotubes had to be produced separately (i.e., not directly on substrates), purified [106, 107], and then manipulated onto substrates before use. At that time, most CVD-grown nanotubes were "spaghetti-like" and largely defective, but the potential of the technique to satisfy technological requirements was recognized. From 1998 onward, substantial and rapid progress was made in the development of CVD to establish it as a highly controlled technology for the production of carbon nanotubes and nanofibers: today, it is possible to fabricate high quality single wall carbon nanotubes [108, 109] or multiwall carbon nanotubes [110], horizontally [111, 112] or vertically aligned [113–115], as an individual nanotube [116–118] or "en masse" [110, 119], with controlled diameter [120, 121] and length [122, 123], structurally as a tube or stacked layered nanofiber form [5, 124], directly onto substrates or in bulk as a raw material [4, 125]. A major advantage of CVD is that the nanotubes/nanofibers can be used directly without further purification unless the catalyst particle is required to be removed, methods for which will be discussed later.

The rest of this chapter discusses the growth mechanism of carbon nanotubes and nanofibers, the various methods of catalyst preparation, and variations in the chemical vapor deposition technique. This provides the technologist with a repertoire of techniques from which he/she can choose the most suitable one for his/her specific application.

2. GROWTH MECHANISM OF CARBON NANOTUBES AND NANOFIBERS

2.1. General Mechanisms

In general, carbon nanotube and nanofiber growth by the catalytic CVD method require catalyst nanoparticles (usually Fe, Co, or Ni), a carbon feedstock (e.g., hydrocarbon or CO), and heat. The diameter of the filament produced is often closely related to the physical dimension of the metal catalyst. The peculiar ability of these transition metals to form graphitic carbon is thought to be related to a combination of factors that include their catalytic activity for the decomposition of volatile carbon compounds, the formation of metastable carbides, and the diffusion of carbon through the metal particles [126]. We present some of the growth models that have been proposed both for nanotubes and nanofibers which are widely accepted by the research community.

The most commonly accepted mechanism was postulated by Baker et al. in the early 1970s, who explained the growth of carbon filaments by catalytic decomposition of the carbon feedstock and bulk diffusion of carbon [1]. According to this mechanism (Fig. 2a), the hydrocarbon gas decomposes on the front-exposed surfaces of the metal particle to release hydrogen and carbon, which dissolve in the particle. The dissolved carbon diffuses through the particle and is precipitated at the trailing end to form the body of the carbon filament. Due to the exothermic decomposition of hydrocarbons, it is believed that a temperature gradient exists across the catalyst particle. Since the solubility of carbon in a metal is temperature dependent, precipitation of excess carbon will occur at the colder zone behind the particle, thus allowing the solid filament to grow with the same diameter as the width of the catalyst particle. Such a process will continue until the leading tip of the catalyst particle is "poisoned" or deactivated. A common cause of catalyst poisoning is the formation of carbon around it, thus preventing the gas from reaching the catalyst particle. Support for this bulk diffusion model comes from experiments on the kinetics of growth of carbon filaments from acetylene (C_2H_2) catalyzed by Ni particles, which yielded an activation energy of (eV) 140 kJ mole^{-1} [2]. This value is similar to the activation energy for bulk diffusion of carbon through solid Ni (i.e., 133 kJ mole^{-1}) [127]. Similarly, the enthalpies for the growth of filaments with α-Fe, γ-Fe, Ni, Co, Fe–Ni, and Cu catalyst were found to be similar to the enthalpy of diffusion. Thus, the rate limiting step in the growth is believed to be the diffusion of carbon through the catalyst. In general, the filament length depends on the duration of the catalytic process, where longer durations result in longer filaments [128, 129]. This general bulk diffusion mechanism accounts for the formation of both nanofibers and nanotubes.

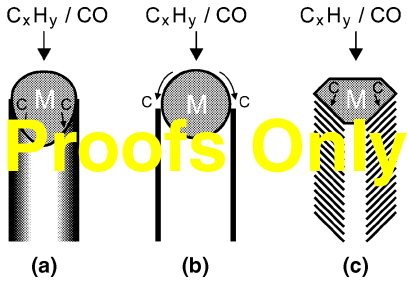

Figure 2. The growth of carbon nanotubes and nanofibers involves the catalytic decomposition of a carbon feedstock (hydrocarbon or CO), carbon diffusion, and its precipitation as a filament. In (a), the carbon diffuses through the bulk of the metal catalyst "M" as proposed by the Baker model [3]. In (b), the carbon diffuses over the surface of the metal catalyst and forms a tubular structure from the circumference of the catalyst as proposed by the Oberlin model [134]. In (c), angled graphene layers are precipitated from a faceted catalyst particle to form a nanofiber as proposed by Rodriguez and Terrones [5, 147].

However, two irregularities of this growth mechanism should be noted. First, not all hydrocarbon dehydrogenation reactions are exothermic (e.g., methane), and yet growth has been observed from these hydrocarbons. Moreover, it is unlikely that there is a temperature gradient across such a small metal particle. This is because the metal particle has a high thermal conductivity and thus a small temperature gradient implies that a massive heat flow is occurring through the particle, which is physically intangible. The exothermic decomposition of the hydrocarbon probably raises the temperature of the entire filament, and the growth of the carbon filament is also probably driven by a concentration gradient of carbon across the particle.

One common question asked is whether the catalyst is a liquid or solid during nanotube/nanofiber growth. If we assume Fe as the metal catalyst, most of the growth experiments are typically well below the melting temperature of iron (1534 °C) and also below the iron–carbon eutectic temperature (1147 °C). The formation of graphite platelets from certain crystallographic faces of the catalyst particle (see Section 2.2) suggests that the catalyst is in a solid form. The agreement between the enthalpy for the growth of filaments and the enthalpy of diffusion for the bulk catalyst metals as discussed earlier also suggests that the catalyst is in the solid phase. Although growth is performed below the eutectic temperature and metal melting point (N.B. usually these temperatures are quoted at 1 atm and will change with operating pressure), one should note that the catalyst metal nanoparticles will behave completely differently than their bulk metal form because these small particles will have exceptionally high surface energy, area, and mobility. For example, Hou et al. reported that annealing iron encapsulated carbon particles in argon between 1000 to 1100 °C completely removes the iron, indicating that these small iron particles were highly mobile at these temperatures [130]. Because of the high mobility and reactivity of the metal atoms, the catalyst nanoparticles are often in the shape of metallic clusters or have been observed to undergo certain surface reconstruction. If temperatures above the metal–carbon eutectic are used, the growth would be similar to the

general vapor–liquid–solid mechanism proposed by Wagner [131, 132] where diffusion through a liquid-phase particle is responsible for the synthesis of filaments.

Instead of bulk diffusion, another common growth model is a catalytic process involving the surface diffusion of carbon around the metal particle [133–135] as shown in Figure 2b. The carbon atoms diffuse over the catalyst surface to form a tubular structure which emanates from the circumference of the catalyst. Note that the tubular structure is favored for carbon filaments with nanometric diameters. A single graphene layer of finite size has many dangling bonds which correspond to high energy states, and for such a small structure, there would be an enormous percentage of dangling bonds if a stacked planar graphite was formed [17, 136]. By the formation of closed tubular carbon shells, the total energy of the system is reduced [136].

An alternative model based on the minimization of surface energy of nanoparticles was suggested by Dai et al. [137]. Nanoparticles contain a very high percentage of surface atoms; as a result a large amount of surface energy exists. Excess carbon can help solve this problem by assembling a graphene cap on the particle surface, called a "yarmulke," with its edges strongly chemisorbed to the metal. Since the basal plane of graphite has an extremely low surface energy (10–20 times smaller than most metals), the total surface energy diminishes. A crucial feature of the yarmulke mechanism was its avoidance at all stages of growth of any open graphene edges, which would expose energetically costly dangling bonds. It also provides an automatic solution to forming caps and resulting structures are tubes which have no seams. Carbon can add to the cylindrical section of a growing layer. Once the smallest yarmulke has formed, insertion of new carbon between the tube edge and the catalytic particle is the best solution, as long as complete overcoating of the particle (i.e., encapsulation) is avoided which would deactivate it.

The actual composition of the active catalyst particle is a widely debated issue, and further research could be performed in this area. High carbon content carbides were determined to be a prerequisite for carbon fiber growth [138–140]. However, there are many conflicting reports concerning the actual composition of the catalyst particle; for example, in the case of an iron catalyst, a hexagonal form with composition $Fe_{2.2}C$ or Fe_2C was postulated, rather than Fe_3C [134]. There are also arguments as to whether a carbide particle is indeed the active catalyst [103]. These are based on the findings that the loss of catalytic activity of iron was accompanied by a gradual conversion of the catalyst to a stable carbide. The catalyst could be reactivated by treatment with hydrogen, reducing the carbide back to iron.

2.2. Nanofiber Growth

Let us now focus our discussion on catalysts used for nanofiber growth and why nanofibers form. The ability to control and tailor the structure of nanofibers (stacked or herringbone) has been demonstrated by Rodriquez et al. [5, 124]. The general concept used here is the creation of a faceted catalyst particle [5, 124, 141] so that carbon feedstock decomposition occurs at certain faces whereas carbon precipitation (in the form of graphite layers) occurs at other faces as shown in Figure 2c. The graphitic platelets are precipitated parallel to the surface of the faceted catalyst particle, and hence the angle between the planes and the fiber axis is determined by the shape of the catalyst particle, as proposed by Boellard et al. [138]. Under certain conditions of gas composition, temperature, and catalyst composition, the catalyst particles undergo surface reconstruction to form unique geometrical shapes which drive the formation of nanofibers [5, 124, 142, 143]. For example, the herringbone structure was found to grow from Fe–Cu (7:3) particles in a C_2H_4–H_2 (4:1) gas mixture at 600 °C, whereas the stacked structure formed from Fe-based catalyst in a CO–H_2 (4:1) gas mixture at 600 °C [5]. The formation of herringbone structures is favored when the catalyst particle is an alloy [124, 144–146], although Pd has also been used alone under certain growth conditions to yield similar structures [147]. Nolan et al. [148] have suggested that hydrogen plays a significant role in the formation of nanofibers. This is because the presence of hydrogen in abundance can terminate the large number of dangling bonds at the edges of the stacked graphite platelets, whereas without hydrogen termination, the more stable form of the carbon filament would be closed tubular graphene shells where there are no dangling bonds. In plasma enhanced CVD, the carbon filaments formed are often nanofibers rather than nanotubes. This is thought to be due to the large amount of atomic hydrogen formed in the gas phase due to plasma decomposition of the hydrocarbon gas or the use of hydrogen as a dilution gas. Delzeit et al. showed that by controlling the relative amount of hydrogen in the gas phase via altering the plasma parameters, one could change the structure from nanotubes to herringbone nanofibers, with high hydrogen content favoring the latter [149].

2.3. Multiwall and Single Wall Nanotube Growth

Let us now concentrate on the formation of nanotubes. Without an abundance of dangling bond terminating species (e.g., H) in the gas phase, carbon nanotubes will tend to form when the diameter of the filaments is ~50 nm or less. This is because a single graphene layer of finite size has many dangling bonds, and these dangling bonds correspond to high energy states [17, 136]. The total energy of a small number of carbon atoms is reduced by eliminating these dangling bonds, even at the expense of increasing the strain energy, thereby promoting the formation of the closed tubular structure [17, 136, 150]. The catalytic activity of the metal catalyst in the formation of nanotubes has also been studied in considerable detail. Besides the commonly used Fe, Co, and Ni catalysts, other metals (such as Mo, Cu) or metal mixtures (Fe–Ni, Fe–Mo, Fe–Co, Co–Ni, and Co–Mo) have been used for nanotube synthesis [109, 113, 122, 128, 137, 151–162]. Using thermal CVD, Co and Fe catalysts generally tend to form hollow and well-graphitized nanotubes, whereas Ni and Cu produced structures which were not as well graphitized [158, 163]. One should note that different metal catalysts would have their optimum catalytic activity at different temperatures [128, 129, 163]. The yield and crystallinity of nanotubes can be improved by the use of metal

catalyst mixtures such as Co–Fe or Co–Ni [158, 164]. Furthermore, it has also been reported that the addition of Mo to Fe or Co [109, 122, 151–157] increases the yield of single wall nanotubes compared to when a single metal catalyst is used [161]. A Co to Mo ratio of 1:2 is reported to be optimal for a high synthesis yield of single wall carbon nanotubes.

Figure 3 shows various forms of nanotubes. Here, the nanotubes are examined using transmission electron microscopy and hence we are looking at a cross section of the nanotubes. The solid black lines in the micrographs represent the hexagonal sheets of carbon atoms which make up the walls of the nanotubes. Under ideal growth conditions, the nanotubes produced should be straight (e.g., Fig. 3a) and contain graphene walls parallel to the tube axis without any defects. Dai proposed that a high growth temperature is required to anneal out defects so that well-crystallized and straight nanotubes could be obtained [165]. The occurrence of defects (e.g., pentagons or heptagons) would cause the nanotube to bend during growth. When carbon nanotubes are formed by the electric arc or laser ablation, temperatures of ~3000 K are obtained and this possibly explains why mostly straight and well-crystallized nanotubes are obtained from these processes. In lower temperature CVD processes (~700–1400 K), "curly" and "coiled" nanotubes (Fig. 3b) are common variations to the perfectly linear nanotube. The growth of various shapes of nanotubes, especially wavy and helical tubes, was investigated by Amelinckx et al. [166]. The concept of a spatial velocity was introduced to describe the extrusion of carbon from the catalyst particle to form the nanotube. Essentially, when the extruded carbon material was uniform, straight nanotubes are obtained, whereas nonuniform extrusion caused the nanotube to deform elastically into complicated patterns such as the helix shape. Nanotubes containing bamboo compartments are also commonly observed, as shown in Figure 3c. A growth model for bamboo-shaped carbon nanotubes was proposed by Lee and Park [167]. Their transmission electron microscopy (TEM) evidence showed that the bamboo-shaped compartment layers were due to the surface geometry of the catalyst particle and the precipitation of carbon sheets from the bulk of the catalyst particle. Li et al. found that when using a higher deposition pressure of carbon feedstock, the nanotubes became bamboo in structure [168]. They argued that at high pressures, the carbon concentration was sufficiently high to cause bulk diffusion of carbon through the catalyst, forming the bamboo compartments behind the catalyst particle. In the literature, bamboo structures are sometimes called "nanofibers." However, note from Figure 3c that the bamboo structure actually contains graphene walls parallel to the filament axis, which suggest that these structures would inherit the physical properties of the "nanotube." It is possible to obtain the growth of straight nanotubes by close-packed growth, use of porous templates, electric field directed growth, or plasma-induced alignment as will be discussed later.

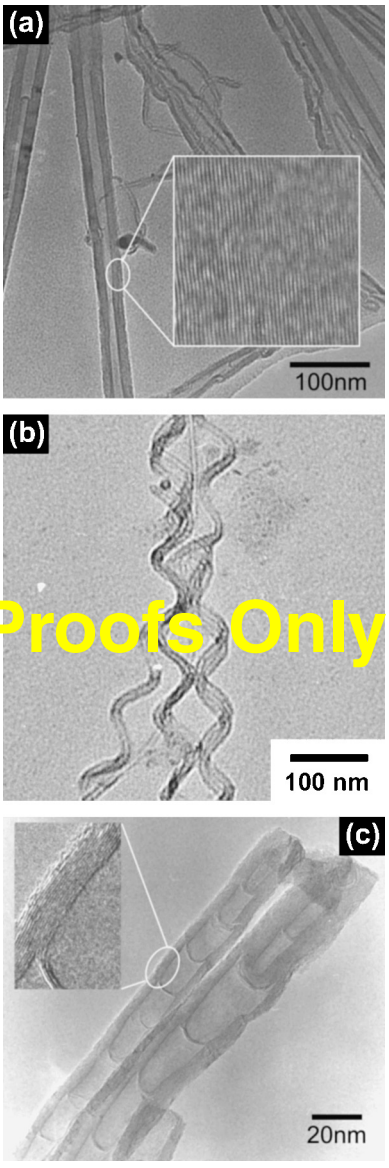

Figure 3. (a) TEM of straight nanotubes grown from the floating catalyst method using ferrocene–toluene at 760 °C. (b) Helical nanotubes grown from CVD of C_2H_2/Ar at 700 °C with Ni catalyst. (c) Straight nanotube with bamboo compartments grown by plasma enhanced CVD of C_2H_2/NH_3 at 700 °C with Fe catalyst.

Under what conditions is the growth single wall carbon nanotubes preferred? The size of the catalyst is probably the most important parameter for the nucleation of single wall carbon nanotubes. Conclusive evidence on the dependence of catalyst size on the formation of single wall carbon nanotubes has been reported in [159, 160, 169]. Li et al. (Duke University) prepared catalyst nanoparticles of uniform diameters (between 3 to 14 nm) by thermal decomposition of metal carbonyl complexes using a mixture of long-chain carboxylic acid and long-chain amine as protective agents [169]. Their results indicate that the upper limit for single wall nanotube growth occurred at catalyst sizes between 4 and 8 nm. Above 8.5 nm, no more single wall structures were observed [169]. Li et al. (Stanford University) also grew single wall carbon nanotubes from discrete catalytic nanoparticles of various sizes [159]. Discrete nanoparticles were prepared by placing a controllable number of metal atoms into the cores of apoferritin. Their TEM studies indicated that the nanotube diameters were closely correlated to the size of the catalytic nanoparticles.

Furthermore, the nanotubes grew by a base-growth mechanism with the nanoparticles seen to be anchored to the support material. Smaller nanoparticles ($<\sim$1.8 nm) were more active in producing single wall nanotubes, while nanoparticles with diameters of $\sim$7 nm did not show single wall nanotube growth, consistent with the group at Duke University [169]. Cheung et al. prepared monodispersed nanoclusters of iron with diameters of 3, 9, and 13 nm [160]. After growth using C_2H_4, single wall and double wall nanotubes were nucleated from the 3 and 9 nm diameter nanoclusters, whereas only multiwall nanotubes were observed from the 13 nm nanoclusters. These works clearly suggest that single wall nanotubes are favored when the catalyst particle is $\sim$5 nm or less. However, it is worth mentioning that there are reports which suggest that single wall carbon nanotubes can be grown from larger catalyst particles. One hypothesis put forward was that bundles of nanotubes could be precipitated from a single larger metal particle and that the bundle formation would be linked to the nature of the metal surface [161]. Note that when arc discharge and laser ablation are used to synthesize nanotubes, bundles of single wall nanotubes are commonly observed to emerge from a large catalyst particle [6]. There is a report of single wall nanotubes grown from $\sim$10 nm diameter colloids, suggesting that the size of the metal nanoparticles may not need to be the same as the diameter of the nanotube [170]. Such reports, however, are rare for the case of CVD and in general, the diameters of the nanotubes and nanofibers grown are often correlated with the size of the catalyst particle.

As mentioned earlier, binary catalyst mixtures have also been reported to increase the yield of single wall carbon nanotubes. A mixture of Co and Mo gives a higher yield of single wall nanotubes than if a single metal catalyst is used [154, 155]. Using X-ray absorption spectroscopy, it was found that Co, originally in an oxide state, is gradually reduced to a metal whereas Mo transformed to its carbide after growth. The role of Mo in the catalyst is to stabilize the small particles of oxidized cobalt species (Co^{2+}), which are highly active for the production of single wall carbon nanotubes [155, 156]. Adding a small amount of Mo to Fe catalyst also increases the yield of single wall nanotubes [152, 153, 171].

Another common observation is that single wall nanotubes are produced via the base-growth mechanism [108, 151, 159] (except for the floating catalyst technique discussed later where there is no base support material). The base growth model is based on TEM evidence which shows that the nanotube tip ends are particle free. Multiwall nanotubes are commonly deposited by both the tip-growth and base-growth mechanisms (see later).

The choice of the carbon feedstock also affects the growth of carbon nanotubes. Baker and Harris [104] reported that unsaturated hydrocarbons such as C_2H_2 had much higher yields and higher deposition rates than more saturated gases (e.g., 100 times that of C_2H_4). They also observed that saturated carbon gases tended to produce highly graphitized filaments with fewer walls compared with unsaturated gases. Thus, hydrocarbons such as methane and carbon monoxide are commonly used for single wall carbon nanotube growth [108, 137, 154–156, 172] whereas hydrocarbons such as acetylene, ethylene, and benzene, which are unsaturated and thus have high carbon content, are typically used for multiwall carbon nanotube growth [122, 129, 158, 164, 173–175].

Hafner et al. further suggested that the growth rate of single wall nanotubes is limited by the carbon supply to the catalyst particles, whereas for multiwall nanotubes, the growth is limited by the diffusion of carbon through the catalyst particle [109]. The authors demonstrated that single wall carbon nanotubes could in fact be grown from a highly diluted gas mixture of C_2H_4. A limited carbon supply will likely allow the structures to form more slowly, giving each carbon atom more time to anneal to its lowest energetic configuration as shown by energetics calculations. Cheung et al. reported that the partial pressure of C_2H_4 had to be increased accordingly in order to nucleate nanotubes from larger nanoclusters [160].

Methane is commonly used as the carbon source for single wall carbon nanotube growth because it is a kinetically stable hydrocarbon and undergoes the least pyrolytic decomposition at high temperatures, typically 900 °C [108, 137]. A small amount of hydrogen or benzene present in the methane flow can enhance the growth yield, as discussed in [176, 177], but too much of these additives impede nanotube growth. Recall that high temperatures are favored for less defective and well crystallized nanotubes, and hence it is important to select a hydrocarbon which does not thermally decompose to form unwanted amorphous carbon (i.e., lower the purity of nanotubes) at high temperatures. Similarly, CO has been used to grow single wall nanotubes at elevated temperatures [172].

Lastly, although it is possible to control the filament structure to obtain nanofibers, multiwall nanotubes, or single wall nanotubes, at the writing of this chapter it is not possible to control the chirality (i.e., electronic properties, either metallic or semiconducting) of the single wall nanotubes through synthesis.

In some applications, the catalyst which was used for growth is not desired. This can be removed by oxidation (to remove carbon layers which may have encapsulated the catalyst particle after growth) followed by acid treatment, similar to what is usually done to purify arc discharge or laser ablated nanotubes [106]. For nanotubes or nanofibers which are tip grown (i.e., catalyst on top), plasma etching could also be used to remove the catalyst particle [178]. It is also possible to run the catalyst back down the nanotube and hence open it by exposing it to hydrogen after growth [3].

Now that we have discussed the growth of carbon nanofibers, multiwall nanotubes, and single wall nanotubes, we shall describe the practical processes for preparing the catalyst and the chambers used for growth.

3. CATALYST PREPARATION

3.1. Growth of Nanotubes/Nanofibers on Substrates

The first step is to prepare the catalyst nanoparticles—it is worthwhile to remember that it is the size of the nanoparticle which approximately determines the final diameter of the nanofiber/nanotube (in some cases also whether a single wall or multiwall nanotube is formed). Hence,

for some applications, it will be necessary to control this parameter. There are several routes for catalyst preparation depending on the final application of the nanotubes. Let us first examine substrate growth or "supported catalyst" growth. There are essentially two reasons to use substrate growth. First, for some applications, it is desirable to coat nanofibers/nanotubes directly onto a particular surface. For example, when carbon nanotubes or nanofibers are used as field emission electron sources for vacuum microelectronic applications, it is desirable to deposit the nanotubes/nanofibers directly within gated apertures to ensure that the structures are as close as possible to the gate so that low operating voltages may be obtained [45, 46, 54, 179–181]. Second, for the large-scale production of nanotubes, it is desirable to anchor the metal catalyst firmly to a support to impede the formation of larger catalyst clusters. Large catalyst clusters are the result of the sintering/coalescence of the metal catalyst particles due to the high surface mobility of the metal atoms and their strong cohesive forces. At the growth temperature, typically 500 to 900 °C, these metal catalyst particles have sufficient mobility to coalesce into larger particles. This effect is especially unwanted if structures of a particular diameter or small diameter (e.g., single wall nanotubes) are required.

Two different growth modes (Fig. 4a and b) can result based on the interaction of the catalyst with its support as described by Baker [3] and Rodriguez [124]. The interaction of the catalyst with the support can be characterized by its contact angle at the growth temperature, analogous to "hydrophobic" (weak interaction) and "hydrophilic" (strong interaction) surfaces. For example, Ni on silica (SiO_2) has a large contact angle (i.e., weak interaction) at 700 °C and thus tip growth is favored in this system [182] as shown schematically in Figure 4a. On the other hand, it is reported that Co or Fe on silicon [110, 183, 184] favors base growth (Fig. 4b), indicating that a strong interaction exists between Co or Fe and Si. Thus, the surface interaction between the catalyst and its support is an important consideration which dictates the growth mode.

Furthermore, one should consider the chemical interaction between the catalyst and its support material which can vary for different temperature ranges. The support/substrate

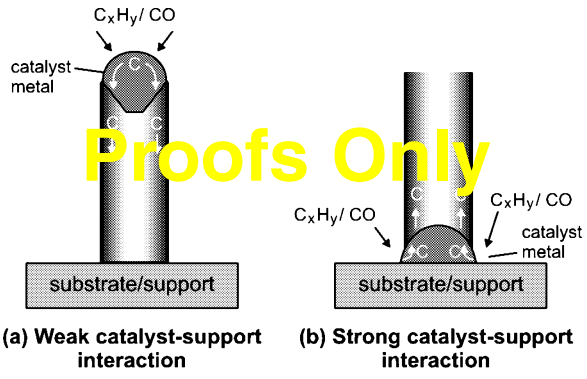

Figure 4. Two types of growth, namely tip or base growth, resulting from different catalyst–support interactions. Adapted with permission from [3], R. T. K. Baker, *Carbon* 27, 315 (1989). © 1989, Elsevier Science.

should not react or alloy with the catalyst at the growth temperature. This is because the catalyst can be "consumed" by the support/substrate if such a reaction occurs. Typical support materials are alumina and silica, which are stable at the range of temperatures used for nanotube growth [152, 153, 155]. Recently, however, much work has focused on the use of silicon substrates in order to reap the benefits of silicon processing to create nanotube electronic devices. Co, Fe, and Ni are known to diffuse into silicon at temperatures near those used for nanotube growth. For example, poor growth yield (or no growth) occurs when Ni catalyst is deposited directly on cleaned Si and reacted with acetylene at 700 °C. This is because Ni diffuses into the Si to form $NiSi_X$ at temperatures above 450 °C [185]. To achieve high yield and uniform growth on Si substrates using Ni catalyst, a diffusion barrier (sometimes called a buffer layer) such as a thin insulating SiO_2 layer (~8 nm) or a conductive titanium nitride (TiN) layer (~20 nm) is used to support the Ni on the Si substrate [186, 187]. On the other hand, Co and Fe are known to have higher diffusion temperatures with silicon [185] and so they can be directly used on silicon substrates at ~700 °C [110, 183, 184]; however, the use of a diffusion barrier (e.g., TiN or SiO_2) is still recommended with these catalysts as it can significantly improve the nanotube yield [188]. This example illustrates the need for careful selection of the catalyst and its support, given the constraints of growth temperature and the particular application of the nanotubes (e.g., on a particular substrate material). Note that a similar problem may arise when Fe/Co/Ni are used directly on metal substrates because the metals may form an alloy at high temperatures. The solution is again to use a diffusion barrier (e.g., conductive metal nitrides or more stable metals) or lower the growth temperature.

Interestingly, for some applications, it is advantageous to use a support layer which does react with the catalyst so that the yield and density of the resultant nanofibers/nanotubes can be controlled. For example, for field emission applications, a densely packed forest of nanotubes/fibers is undesirable because the screening of the applied electric field from the adjacent nanotubes/fibers reduces the overall geometric field enhancement obtained from the high aspect ratio of the nanotube/nanofiber. Instead, sparsely spread structures, roughly spaced twice their height apart [98–100], overcome field screening problems. The growth of sparsely spread nanotubes/nanofibers is achieved by using an "imperfect" barrier layer which only consumes some of the catalyst, as described in [186].

There are several routes to the production of catalyst nanoparticles, and the most commonly used methods are described in the following sections.

3.2. Wet Catalyst

In the wet catalyst method, a liquid solution containing the catalyst in salt form is applied to the substrate via spray coating [189], spin coating [190], or microcontact printing [191]. Soluble salts are typically used, such as acetates or nitrates (e.g., in [191] iron, nickel, or cobalt nitrates [$Fe(NO_3)_3 \cdot 9H_2O$, $Ni(NO_3)_2 \cdot 6H_2O$, $Co(NO_3)_2 \cdot 6H_2O$]). After application to the substrate, the salt solution is often reduced to oxide nanoparticles by calcination (i.e., heating in air) [192].

Metal oxides are stable and improve the catalyst–support interaction at growth temperature—in some cases, metal oxides are used directly as the catalyst [108]. During growth, these oxides are reduced to metal nanoparticles (e.g., using hydrogen) which catalyze the subsequent growth of carbon nanotubes or nanofibers. Note that catalyst decomposition and reduction can occur as part of the deposition process because the nanotube growth is usually performed at elevated temperatures. The density of the nanotubes/nanofibers is simply controlled by the concentration of the catalyst solution, which is typically in the range of 1 to 500 mM [98]. Selective growth on substrates with wet catalysts often involves the use of inked stamps/molds, inkjet printing onto desired areas, or wet coating of a resist-masked substrate [151].

Mixtures of different metal salts have also been used as catalysts for nanotube growth. The combination of different metal catalysts can enhance the yield of nanotubes as described in the previous section. However, with different combinations of metal salts, it becomes increasingly difficult to find an optimum "recipe." One method to overcome this challenge is to use high-throughput inkjet printing or microarray printing to transfer different catalyst mixtures onto a substrate [193–195]. Microarray printing has the advantage of being relatively low cost when applied over large areas, and it can provide relatively high spot density ($>10^3$ spots per cm^2) and experimental flexibility with different mixtures of catalyst solutions. For example, this method was used to study the effectiveness of different metal salts to determine the optimal catalyst composition for the growth of multiwall and single wall carbon nanotubes [194, 195].

It is also possible to deposit catalyst nanoparticles onto a substrate by electrochemical deposition with a metal salt solution. Tu et al. used a solution of 0.01 M of $Ni(SO_4)$ and 0.01 M of H_3BO_3 to electroplate Ni nanoparticles onto a Si substrate which was metallized with Cr [196]. By changing both the current density and time during electrochemical deposition, it is possible to control the density of the particles and hence the density of the carbon nanotubes on the substrate.

The catalyst support for nanotubes/nanofibers could also be in the form of a powder/nanoparticles (typically alumina, silica, or graphite). In the wet catalyst method, these powders are impregnated with the catalyst [163, 173]. For example, graphite can be impregnated with a 40 vol% ethanol/60 vol% water of iron (III) oxalate to form a 2.5 wt% Fe/graphite sample as described in [173]. This sample was next dried in nitrogen at 250 °C and reduced in hydrogen to form metallic iron which was then used to catalyze the growth of multiwall nanotubes using acetylene at 700 °C. The impregnation method has also been used to prepare catalyst for single wall nanotubes as well [161, 197]. The most promising catalyst that has been reported by such a method is a Co–Mo metal supported on silica as described previously [155, 157]. The impregnation technique is often used for the bulk production of nanotubes and nanofibers. At the end of the reaction, the support can be removed by dissolution in strong acid or alkali to yield the carbon structures.

Another wet catalyst preparation route is co-precipitation which involves the reaction of metal salt solutions with ammonium bicarbonate to form metal carbonates. The metal carbonates can be reduced to metal oxides by calcination [5] and further reduced to the metal catalyst during growth using hydrogen.

Wet catalysts are especially useful for coating nonplanar geometries such as wires or tips [198–201]. These surfaces can either be dipped in the catalyst solution or the solution can be spin-coated onto the substrate.

3.3. Thin Film Metals

Another common technique of depositing the metal catalyst is by physical vapor deposition. A very thin film of Fe, Co, or Ni is carefully deposited on a substrate using sputtering or evaporation. The film thickness is usually in the few nanometer range and is monitored during deposition using a quartz oscillator-type film thickness monitor for accuracy. When this thin film is heated up to a high temperature (such as the growth temperature), the thin film breaks up and coalesces to form nanoclusters due to increased surface mobility and strong cohesive forces of the metal atoms [117, 183]. These nanoclusters then catalyze the growth of the carbon nanotubes or nanofibers. In general, the size of the nanoclusters formed can be controlled by the thickness of the catalyst film [182, 183, 202], by the temperature [203, 204], or by the annealing time. Thicker films, higher temperatures, and lengthy annealing times lead to the formation of larger metal clusters due to increased surface migration of the metal atoms. Although these parameters may be used to control the average size of the nanoclusters (i.e., diameter of resultant nanofibers/nanotubes), one should note that the formation of nanoclusters from the metal film is a random process and thus there will still be a distribution in the diameters of the structures [183, 202].

Multilayer metal films have also been used to catalyze nanotube growth. A noncatalyst metallic underlayer can be used to control the surface properties of the catalyst or the deposition yield as discussed earlier. Single wall nanotubes have been grown using a three layer metal film containing 0.2 nm Mo on 1 mm Fe on 10 nm Al on a silicon substrate [171]. These authors showed that the metal films formed Fe/Mo catalyst particles of ~2 nm diameter which seeded the single wall nanotubes.

The advantage of using catalyst thin films is that they can easily and accurately be patterned by using masking or etching techniques based around photolithography or electron beam lithography. In fact, individual freestanding nanotubes and nanofibers have been deposited using this process [116–118]. Figure 5 shows some examples where a 7 nm thin Ni film was patterned with lines and dots, which were then used to nucleate nanotubes. To obtain single freestanding structures, the Ni film must be patterned into dots of ~300–350 nm or less [117, 205]. When the Ni film dots are heated up to the growth temperature (700 °C), the film forms a single catalyst cluster of equal volume and catalyzes the growth of the nanotube. The vertically standing nanotubes of Figure 5 were deposited by plasma enhanced chemical vapor deposition which will be discussed later.

Note that when the metal film thickness exceeds a few tens of nanometers, nanoclusters are no longer formed and the film forms islands a few micrometers in size. These large

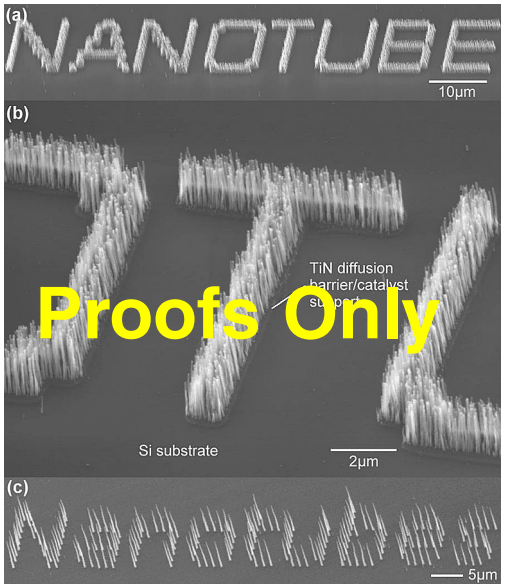

Figure 5. A 7 nm film of Ni catalyst, prepared by sputtering, was patterned using lithography into lines (a,b) and dots (c). The substrate used was Si, and hence a TiN diffusion barrier (also prepared by sputtering) was used to support the catalyst as Ni reacts with Si at the growth temperature. The growth was performed by plasma enhanced CVD of C_2H_2:NH_3 at 700 °C. The nanotubes formed are straight, vertically aligned, and typically bamboo in structure (like the TEM shown in Fig. 3c). Using plasma enhanced CVD, it is also possible to attain slightly conical shaped structures [as in (c)] by altering the synthesis conditions which is described in [268].

micrometer-size islands/particles usually do not catalyze filament growth but instead absorb carbon into their bulk. Nanotube/nanofiber growth is usually found around the grain boundaries of metal islands. This is because smaller (submicrometer) catalyst particles are often present around the grain boundaries. Baker et al. also observed that carbon filament growth occurred only from the edges of macroscopic Fe foil [192]. In this case, the catalyst material probably easily detached at the metal foil edges to form small catalyst particles which nucleated the carbon filaments. Note that large (micrometer-sized) catalyst grains or thick continuous catalyst films do not nucleate nanotubes. The uniform growth of nanotubes inside large metal grains or catalyst metal substrates is only possible if nanoparticles are present on the surface of the metal as described in the next section.

3.4. Thick Metal Catalyst Films or Metal Catalyst Substrates

Nanotubes or nanofibers can be grown with high yield on thick catalyst metal films or catalyst metal substrates when surface treatment techniques are first used to roughen the substrate surfaces. Mechanical roughening or electrochemical etching may be used to generate a coarse surface. Plasma etching or ion bombardment has also been used to increase the roughness of the metal surface and to generate submicrometer metal islands/particles [113, 206–208]. These surface roughening techniques generate the small catalyst particles needed to grow carbon filaments. An alternative technique is to oxidize the metal surface through heating in oxygen or by rusting [192]. During growth, the metal catalyst nanoparticles are formed from the rusty, porous oxide surface by decomposing it with a reducing gas (e.g., H_2).

3.5. Colloids

Colloidal metal (or oxide) particles have also been used to catalyze the growth of nanotubes. Colloids are usually synthesized (or bought) in liquid suspensions where the colloids are separated by adsorbed charged species or organic molecules. The advantage of using colloids is that these can be highly homogenous in size and can be synthesized in diameters down to 2 nm. Thus, the use of colloidal catalysts allows the growth of nanotubes with well defined diameters, in contrast to the other techniques mentioned above which tend to produce a nanotubes with a significant variation in diameter (except for the growth of single nanotubes from a small catalyst patterned dot where the catalyst is essentially fixed in size/volume). Cheung et al. describes the preparation of monodisperse Fe clusters with different diameters and uses these to catalyze the growth of single wall nanotubes supported on an oxidized Si substrate [160]. Li et al. have also synthesized colloids of diameters varying from 3 to 14 nm to catalyze nanotube growth [169]. Colloidal metal suspensions can in general be applied to the substrate using similar techniques as for the wet catalyst. Additionally, colloidal solutions in which the particles are separated by charge can be easily applied to substrates which have been functionalized with oppositely charged surface layers [209].

3.6. Sol–Gel Technique

The sol–gel technique has also been used to prepare catalyst for both multiwall and single wall carbon nanotube synthesis [153, 158]. Sol–gels impregnated with metal catalysts have very high surface area, high porosity, and ultralow density—these characteristics lead to a high yield of nanotubes during growth. For example, a Fe–Mo catalyst was prepared by the sol–gel technique based on supercritical CO_2 drying and then used for single wall carbon nanotube synthesis, as described in [153]. This catalyst was reported to be capable of deposition yield of over 200% compared with the original weight of the catalyst for a 1 hour deposition. The catalyst was active for 6.5 hours of growth, yielding 600% weight gain in total. The high yields were the result of the aerogel having a high surface area, high porosity, and good metal–support interaction. As yet, no other research group has been able to exceed the yields of single wall carbon nanotubes on a supported substrate by sol–gel [153].

3.7. Unsupported/Floating Catalyst Method

The floating catalyst method is commonly used for the bulk/mass production of nanotubes/nanofibers by CVD. The main advantage of using this technique is that purification is not required to recover nanotubes from the substrate. The simplest method is to inject catalyst nanoparticles (e.g., in the form of a colloidal/particle suspension or organometallic precursors with a carbon feedstock) directly into the CVD

chamber. In this case, a vertical CVD chamber is usually used so that the nanotubes/nanofibers grow as the catalyst particles fall from top to the bottom of the chamber. This technique has been used to prepare vapor grown carbon fibers for over 20 years [4, 105, 210–212].

Organometallic compounds are often used as precursors for the catalyst. Examples of organometallic compounds that have been commonly used are metallocenes, iron pentacarbonyl, and iron (II) phthalocyanine [4, 172, 211–219]. These precursors are usually sublimed and catalyst nanoparticles are formed *in situ* when the compound is decomposed/reduced by heat or hydrogen. A double stage furnace is typically needed because of the different temperatures needed for organometallic sublimation and nanotube growth. In general, the sublimation of metallocenes offers little control over the structural parameters of the nanotubes such as length and diameter, although it has been shown that by varying the relative concentration of the metallocene to carbon in the gas phase the average diameter of the structures may be changed [219, 220]. An improvement over the double stage furnace is to use a syringe pump and atomizer to continuously feed a metallocene–liquid carbon feedstock solution into a single stage furnace where nanotube growth occurs [219, 221–223]. Aligned, high yield and pure multiwall carbon nanotubes can be obtained with conversion rates of 25% of the carbon input using this method. Very often, the floating catalyst technique leads to highly dense/close-packed nanotube deposition where essentially only upward (i.e., "aligned") growth of the nanotubes is possible.

Interestingly, the floating catalyst method can also be used to selectively grow nanotubes on substrates [224, 225]. It was observed that multiwall carbon nanotubes grown by CVD of ferrocene and xylene at 800 °C only occurred on silica (SiO_2) surfaces and not on Si surfaces. Thus, by using lithographic means to pattern SiO_2 on a Si substrate, selective growth of nanotubes was obtained [225]. The multiwall nanotubes were aligned and grew perpendicularly from the SiO_2 surfaces. In this case, it was suggested that it was the good catalyst–support interaction between SiO_2 and Fe that led to the growth of nanotubes. If metal layers of nickel (Ni) were patterned onto Si, the nanotubes were seen to lift these metal patterns during growth [226]. Such aligned nanotubes have also been grown on gold and MgO substrates and palladium seeds [227–229].

Typically, metallocene assisted chemical vapor deposition of hydrocarbons (e.g., benzene, xylene) produces multiwall carbon nanotubes at lower temperatures (~700 °C) whereas a combination of multiwall and single wall nanotubes are produced at much higher (>900 °C) temperatures. For example, pyrolysis of iron pentacarbonyl with benzene at 900 °C leads to single wall nanotube formation [220]. Nickelocene and cobaltocene were reported to be more favorable for single wall nanotube synthesis than ferrocene, although no differences in single wall nanotube yields were observed when binary mixtures of metallocenes were used, except that the nanotubes appeared to be "cleaner" when mixtures were used [230].

The addition of trace amounts of thiophene (sulfur containing compound) to liquid hydrocarbons has also been reported to promote the growth of single wall carbon nanotubes [170, 231, 232], although higher concentrations of thiophene were reported to revert the growth back to multiwall in structure (>5 wt%) [170, 231]. Recently, extremely long ropes (several centimeters in length) of high purity single wall nanotubes have been synthesized with the vertical floating catalyst method using a ferrocene, *n*-hexane, and thiophene mixture with hydrogen as the carrier gas [232–234]. These macroscopic ropes will definitely enable the use of single wall nanotubes in mechanical applications.

"HiPCO," developed at Rice University, is also a process involving a high pressure gas phase catalytic process for single wall nanotube growth [172, 235]. The catalyst is formed *in situ* by the thermal decomposition of iron pentacarbonyl in a heated flow of CO, and growth is performed at pressures ranging from 1 to 10 atmospheres (atm) and temperatures ranging from 800 and 1200 °C. The optimum condition for maximum yield was at 1200 °C and 10 atm. The rate at which the reactant gases were heated also had substantial effects on the amount and quality of nanotubes produced. The addition of small amounts of methane (0.7% by volume) produced clean nanotubes and increased the yield as well. Although milligram quantities were obtained, such a process is continuous and is being currently scaled up to produce larger quantities of single wall nanotubes (marketed as HiPCO™ single wall carbon nanotubes by Carbon Nanotechnologies Inc.).

4. CHEMICAL VAPOR DEPOSITION CONFIGURATIONS AND CONSIDERATIONS

4.1. Horizontal Furnace

The horizontal furnace is the most popular configuration for the production of carbon nanofibers and nanotubes [4, 124, 137, 173]. In its simplest form, it is a heated quartz tube in which the substrates/catalyst are placed. The reactant gases are flowed over the substrates/catalyst which sit in a removable ceramic boat/holder in the center of the quartz tube (see Fig. 6a). The horizontal furnace is advantageous because there is no (or small) temperature gradient within the heated zone. In most cases, the length of the nanotubes/nanofibers can be simply controlled by the length of the deposition time.

When samples are first put into the chamber, the quartz tube is first flushed with a "carrier" gas. The most popular carrier gases are argon, hydrogen, and nitrogen [4, 115, 158, 161, 221, 232]. Argon is mostly used as it easily displaces air and therefore easily forms an inert atmosphere in the chamber. The furnace is then heated up to the growth temperature in the inert atmosphere. Hydrogen is often added to the gas flow to reduce the catalyst particles (e.g., oxides) during heating. Even if the chamber is evacuated by a pump, it is important to maintain a forward flow of inert/reducing gases during heating as it is possible that nanotubes may undesirably grow from the catalytic cracking of pump oil (e.g., from back streaming). When the growth temperature is reached, the carbon feedstock is introduced. As discussed in the growth mechanism section, the choice of carbon feedstock and other additives is based on whether nanofibers, multiwall nanotubes,

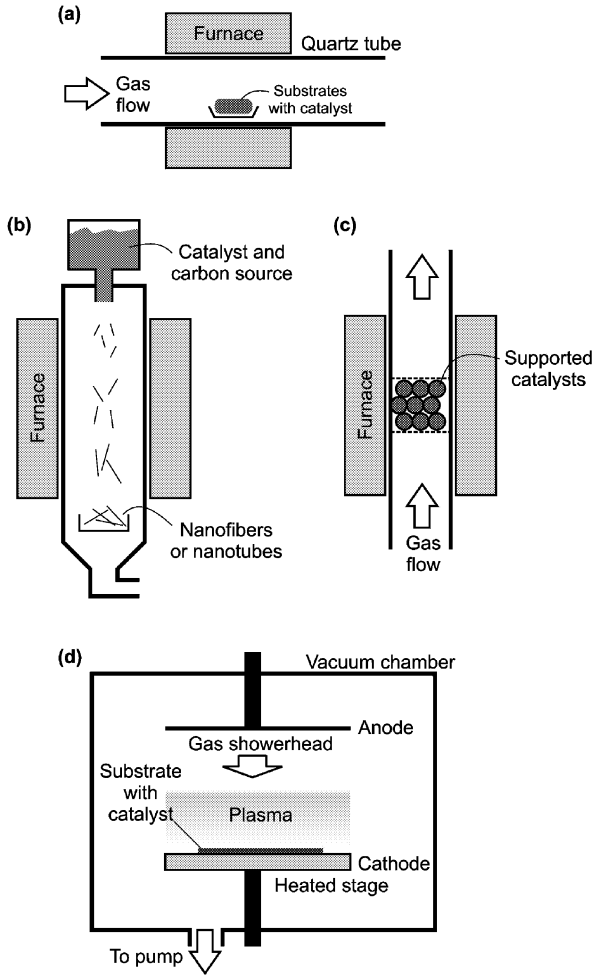

Figure 6. Types of chambers used for catalytic CVD of nanofibers and nanotubes. The most commonly used is the horizontal furnace (a). For mass production, the vertical furnace (b) has been employed. (c) The fluidized bed reactor and (d) a basic plasma enhanced CVD system based around a vacuum chamber.

or single wall nanotubes are desired. Reactions are usually conducted at temperatures below 1000 °C to reduce the formation of undesirable carbon deposits such as amorphous carbon [151]. The amorphous carbon is deposited from the thermal decomposition (pyrolysis) of the carbon feedstock gas, whereas the carbon nanotubes/nanofibers are grown from the catalytic decomposition of the carbon feedstock gas. In most cases, "clean" (i.e., amorphous carbon-free) growth of highly crystallized structures is desired and hence the highest deposition temperature without significant self-decomposition of the carbon feedstock is preferred.

In order to determine the highest growth temperature possible using a particular carbon feedstock, it is necessary to consider the thermodynamic stability of the compound depending on temperature. The driving force for the pyrolytic reactions involving gaseous components can be derived from plots of the free enthalpy of formation versus temperature (generated using [236]) as shown in Figure 7. The term pyrolytic is defined as converting the carbon feedstock to solid carbon as the main product and to different

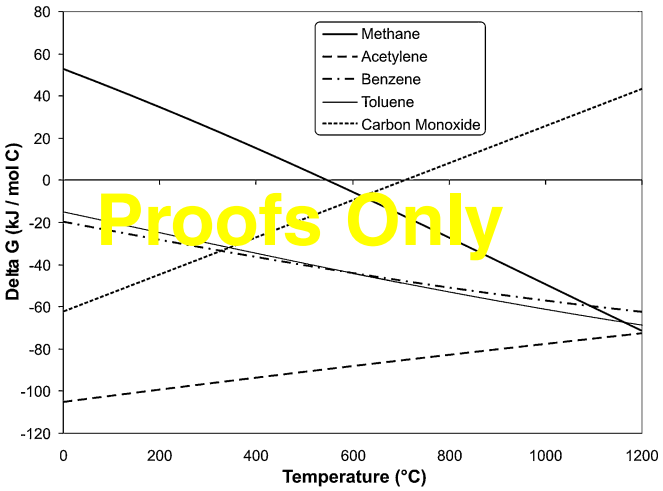

Figure 7. The free enthalpy of formation of some carbon compounds, calculated from [236, 237].

volatile compounds as by-products [237]. The stability of the compound increases with the free enthalpy, whereas the driving force for breaking the compound into its elements decreases. For example, the forward reaction producing elementary carbon from carbon monoxide is favored at temperatures below 700 °C.

In general, there is a compromise between obtaining high purity carbon nanotubes/fibers and high crystallinity. The growth temperature affects the crystallinity of the structure produced, but too high a temperature leads to the formation of pyrolytic amorphous carbon. Furthermore, the diffusion of carbon through the catalyst is a thermally activated process, and hence, in general, higher temperatures lead to higher growth rates which may be desirable for mass-production processes.

One strategy to reduce the formation of amorphous carbon is to decrease the contact time between the carbon feedstock and the substrates. This is achieved by using very high gas flow rates (in cases where only carbon feedstock is used in the flow) or high dilution [129, 163, 175, 238]. Thus, the carbon feedstock is often diluted by the carrier gases. Normally there is an optimum ratio of carbon feedstock to carrier gas; for example, using acetylene and nitrogen, the optimized combination was 9% by volume of the total gas flow. If the acetylene combination is increased, amorphous carbon begins to form due to the self-pyrolysis carbon feedstock and the increased exposure of the sample to the carbon feedstock [129].

A small amount of hydrogen in the gas flow is useful in keeping the catalyst particle active by reducing it. It is well known that the growth of nanofibers is enhanced in a hydrogen atmosphere [4, 148, 189, 239]. Hydrogen also reduces the formation of undesirable carbon deposits from the pyrolysis of carbon feedstock [159]. This is because hydrogen rehydrogenates the reactive carbon species in the gas phase. Franklin et al. found that for clean single wall carbon nanotube growth at 900 °C, the optimum flow of hydrogen was between 100 and 150 ml/min in a predominantly CH_4 flow (CH_4 = 1500 ml/min) [176]. The flow of hydrogen had to be increased to 200 ml/min to maintain

"clean" growth if a temperature of 950 °C was used. In the absence of hydrogen flow, the CH_4 was found to pyrolyze and form amorphous carbon deposits all over the substrate.

Alternatively, the floating catalyst method can also be used in the horizontal furnace configuration for carbon nanofiber or nanotube growth [4, 212]. As discussed before, the catalyst can be sublimed in a preceding furnace stage and flowed into the main furnace for growth or injected directly into the growth furnace using a syringe pump or atomizer spray [4, 213–219, 221–223, 240]. The growth of nanotubes would then occur all over the walls of the quartz tube and also on any substrates placed inside the furnace. This technique is very useful for bulk production since the material can simply be removed from the walls of the chamber or from the substrates after growth. Note that selective area growth is also possible with the floating catalyst technique by using different substrate materials; for example, SiO_2 supports nanotube growth whereas Si does not [224, 225].

Finally, note that a furnace is not necessarily required to generate the heat needed for nanotube growth. It is possible to grow nanotubes on wires through direct heating with electrical current [241]. Furthermore, plasma or radio-frequency (rf)-induced heating of the catalyst particle can also generate sufficient temperature locally for carbon nanofiber/nanotube growth at lower process temperatures [242].

4.2. Vertical Furnace

The vertical furnace configuration, as shown in Figure 6b, is usually employed for the continuous production of carbon fibers, nanofibers, and nanotubes [4, 125, 211, 232, 243]. The catalyst and carbon source is injected at the top of the furnace and the resultant filaments grow during flight and are collected at the bottom of the chamber. The vertical furnace can be run continuously for the mass production of carbon nanotubes and nanofibers. Ultrafine metal catalyst particles are either introduced into the reactor directly or formed *in situ* using precursors such as metallocenes as discussed previously. Note that the residence time of the catalyst particle in the vertical furnace is relatively short compared to the horizontal furnace.

As discussed earlier, the growth of multiwall or single wall nanotubes is dependent on the temperature and gases used, with higher temperatures and the addition of a sulfur containing compound (e.g., thiophene) favoring single wall nanotube production [170, 231, 232]. The main advantage with the vertical furnace configuration is the continuous nature of nanofiber/nanotube production and high purity product eliminating the need for purification or removal from the substrate. The vertical furnace technique has been commercialized for the production of multiwall nanotubes and nanofibers, in quantities of tons per year. Most of this material is used in the electrodes of lithium-ion batteries [73] and as fillers in conductive polymers [35].

The fluidized bed reactor (Fig. 6c) is a variation of the vertical furnace. Fluidization is defined as the transformation of solid particles into a fluidlike state through suspension in a gas or liquid. As seen in Figure 6c, supported catalysts are usually placed in the center of the furnace and an upward flow of carbon feedstock gases is used. The fluidization process involves the supported catalysts to remain much longer in the furnace than in the vertical floating technique. The fluidization method is relatively new for the bulk production of carbon nanotubes [244–246], and thus far, production rates up to tens of kilograms of multiwall carbon nanotubes a day have been achieved [244].

4.3. Aligned and Directed Nanotube Growth

In some applications, the deposition of well aligned carbon nanotubes or nanofibers on substrates is desired. In this area, chemical vapor deposition is uniquely superior to the other nanotube production techniques (i.e., electric arc discharge and laser ablation) in that nanotube/nanofiber alignment on substrates is readily achievable during growth. Whenever very dense and closely packed nanotubes are deposited (see Fig. 8a), they are forced to grow in an upward ensemble (i.e., perpendicularly) from the substrate—this is sometimes referred to as "self-oriented" or "self-assembled" growth. It is generally believed that the nanotube ensemble is held together by van der Waals interaction and that the nanotubes are so closely packed that the only possible

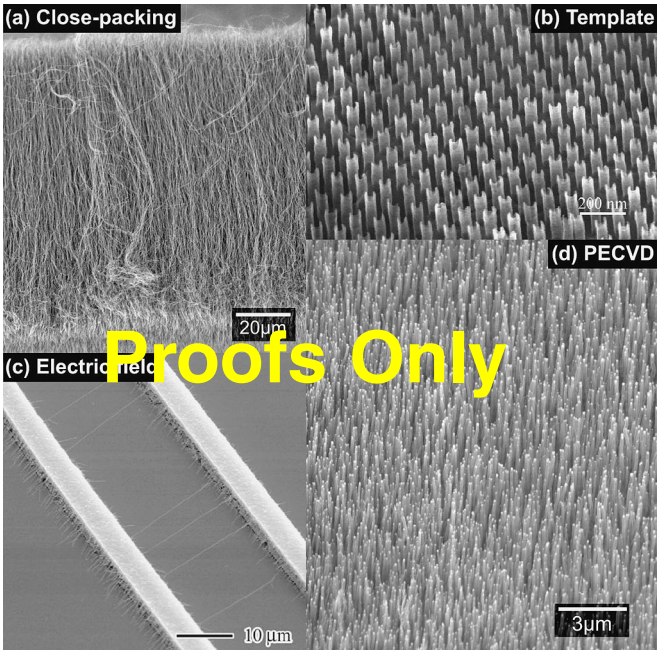

Figure 8. Methods of aligning nanotubes during growth. In (a), densely packed nanotubes grow approximately vertically aligned, as shown in this peeled section of a nanotube "film." This was deposited using the floating catalyst technique employing a ferrocene–toluene solution injected into a heated furnace (750 °C). In (b), perfectly straight, same diameter, and same length nanotubes are grown in the pores of a nanochannel alumina template. In (c), a lateral electric field of 0.5 V/μm is used to guide these single wall nanotubes horizontally between electrodes during growth. In (d), straight, vertically aligned carbon nanotubes were grown using plasma enhanced CVD. It is believed that the electric field in the plasma sheath which forms over the substrate aligns the structures during growth. (b) Reprinted with permission from [250], J. Li et al., *Appl. Phys. Lett.* 75, 367 (1999). © 1999, American Institute of Physics. (c) Reprinted with permission from [111], Y. G. Zhang et al., *Appl. Phys. Lett.* 79, 3155 (2001). © 2001, American Institute of Physics.

growth direction is upward. Thus, the key factor in achieving this type of dense, aligned growth is the preparation of dense and active catalyst particles on the substrate surface. One of the most spectacular examples of this was reported by a Chinese research group [114, 119]. The authors prepared iron oxide nanoparticles in the pores of mesoporous silica, which was then reduced to iron particles by H_2/N_2 flow at 550 °C, followed by reaction with C_2H_2 at 700 °C for nanotube growth. Dense arrays of nanotubes grew perpendicularly outward from the mesoporous silica, and bundles of nanotubes up to 2 mm in length were synthesized [119].

Fan et al. also synthesized "towers" of densely packed nanotubes by using a 5 nm thin film of evaporated iron on electrochemically etched porous silicon [110]. The authors explained that during growth, the walls of the nanotubes interact with their neighbors via van der Waals to form a rigid bundle during growth. In fact, close examination of these nanotube "towers" revealed that there were no nanotubes which "branched out" from the main tower. As the catalyst was rooted at the base of the structure (i.e., base growth), the porous substrate played a key role in the growth as it allowed the deposition gas to continuously feed the catalyst. The strong interaction between the substrate and the catalyst also meant that the catalyst was well rooted and did not sinter to form larger catalyst particles at the growth temperature. Dense and aligned nanotube growth on substrates has also been observed with evaporated iron on oxidized Si [167], from laser-ablated Co catalyst on silica substrates [115], and from substrates coated by nanotubes from the floating catalyst method as discussed earlier [218, 220, 221, 225]. In general, the close-packed nanotubes are not perfectly straight and exhibit some degree of waviness as seen in Figure 8a.

Another common means of achieving aligned growth is through the use of templates, the most popular of which are vertical nanopores created by the electrochemical processing (anodization) of aluminum. Porous alumina membranes typically contain vertical nanopores which are a few to hundreds of nanometers in diameter and lengths which can range from a few micrometers to hundreds of micrometers. The electrochemical parameters can be varied to control the pore diameter, length, and density—a review of the template preparation and growth of nanomaterials is given in [247]. The intent is to grow nanotubes within the alumina pores so that the diameter, length, density, and alignment of the structures reflect that of the original template. The use of porous alumina in the synthesis of carbon nanotubes was first reported in 1995 [248]. In general, two types of template grown structures are possible, namely catalyzed and pyrolytic (no catalyst). The latter usually requires higher temperatures in order to decompose the carbon feedstock gas. Che et al. prepared carbon nanotubes with diameters ~20 nm using an alumina template in ethylene/pyrene with a Ni catalyst at 545 °C or without catalyst at 900 °C [249]. After growth, the alumina template can be removed by dipping in HF or NaOH solution to reveal an array of well-ordered carbon tubules standing perpendicular on the substrate. Figure 8b shows what is possible with this technique—a well-aligned, hexagonally packed nanotube ensemble with highly homogenous diameter and lengths. This was prepared by Li et al. using an alumina template together with Co/Ni catalysis of acetylene at 650 °C [250]. The smallest nanotubes, 4 Å (0.4 nm) in diameter, have been fabricated using zeolite templates [251].

Another strategy of obtaining vertical nanotube/nanofiber growth is through the use of electric fields. Avigal et al. used a vertical electric field during growth to achieve vertical alignment of nanotubes [252]. A similar effect arises during plasma enhanced chemical vapor deposition (see Fig. 8d) which is discussed in the next section.

The above techniques yield the growth of vertically aligned structures—but what about horizontally aligned ones? Horizontally aligned nanotubes are necessary for the mass production of nanotube electronic and spintronic devices. The group led by Dai, at Stanford University, is a pioneer in this area. In their early work, straight, single wall nanotubes were grown from patterned catalyst but in random directions [151]. In some cases, the nanotubes grew in the correct direction (e.g., between electrical contacts) which allowed the fabrication of nanotube electronic devices [63, 253, 254]. Clearly there was a need to control the growth direction in order to achieve a higher fabrication yield of nanotube devices. In [177], they fabricated silicon pillars and contact printed the catalyst for single wall nanotubes on top of the pillars. A suspended network of nanotubes was observed from the pillars after growth. Fascinatingly, the direction of the suspended nanotubes followed the pattern of the pillars—for example, when the pillars were lined up in rows, nanotubes would be found to be suspended from the pillar tops resembling a power line. Using this technique, 100–150 μm long single wall nanotubes were grown. If four pillars were arranged in a square, a square arrangement of suspended nanotubes would join the tops of the pillars. The authors reasoned that the nanotubes growing toward a pillar would adhere to the pillar and become suspended, whereas nanotubes growing in other directions do not meet a pillar and would fall down toward the substrate. Thus, the arrangement of pillars essentially defined the growth direction of the nanotubes.

Lateral electric fields can also be used to guide nanotubes during growth. Zhang et al. prepared electrode and catalyst "fingers" on a quartz substrate which were biased during chemical vapor deposition in order to create a lateral electric field [111, 112]. The authors found that electric fields of 0.13–0.5 V/μm were needed to guide and align the single wall nanotubes during growth, as shown in Figure 8c. The mechanism of alignment was due to the electric dipole polarization of the nanotubes which made them align in the applied electric field.

Lee et al. also presented a technique for the directed growth of lateral nanotubes. These authors made a sandwich structure comprised of SiO_2–Ni–Nb on silicon [255]. Using microfabrication, only one face of the sandwich was left exposed to the gases and it was from this face that the Ni catalyzed the outward/lateral growth of multiwall nanotubes in C_2H_2/N_2 at 650 °C.

4.4. Plasma Enhanced Chemical Vapor Deposition

Plasma enhanced chemical vapor deposition (PECVD) is a relatively new technique of producing vertically aligned carbon nanotubes and nanofibers, and it is considerably

different from the horizontal and vertical furnace techniques. A plasma is an excited/ionized gas, and the processing plasmas, usually known as "cold" plasmas, are generated using dc, rf, or microwave excitation. The simplest plasma system to implement is the dc plasma which is shown in Figure 6d. The dc glow discharge plasma is generated by grounding the anode and applying a dc negative bias of 400–600 V onto the cathode (note that the substrate for nanotube/nanofiber growth is on the cathode in this case such that the plasma would form a sheath over it with a large voltage drop). Plasma systems are commonly used in semiconductor processing for etching or low temperature deposition of thin films. A review presenting the different configurations of plasma systems is presented in [256]. Today, carbon nanotube/nanofiber growth has been demonstrated with hot filament assisted PECVD [113, 206–208], microwave PECVD [257–262], dc glow discharge PECVD [117, 182], inductively coupled plasma PECVD [74, 149], and rf PECVD [242, 263]. Plasma depositions are very stable—this leads to highly controllable and reproducible growth conditions. PECVD is usually used to produce vertically aligned carbon nanotubes/nanofibers or grow nanofibers at low temperatures.

Chen et al. used a combination of hot filament and dc PECVD (via negative bias on the substrate) to grow aligned carbon nanofibers using a single crystal Ni$\langle 100 \rangle$ surface with CH_4 and N_2 gases [206]. This process was later refined using 3% C_2H_2 in N_2 and a polycrystalline Ni substrate to grow nanofibers of 60–70 nm average diameter and few micrometers in length [207]. The structures produced by Chen et al. were classed as nanofibers because their TEM showed that the graphene planes were slightly tilted/herringbone, although the nanofiber was hollow in the center. These films showed excellent field emission characteristics with low turn-on electric fields and high emission currents.

A major application for carbon nanotubes is the electron source in field emission displays (a flat panel display technology). The major drawback, however, is that nanotube growth typically requires temperatures of 700 °C or higher which exceeds the strain point of the best "display" glass (by Corning) of 666 °C. Hence, there was great excitement in 1998 when Ren et al. demonstrated that vertically aligned carbon nanotubes could indeed be deposited below that temperature on glass, using hot filament assisted dc-PECVD of C_2H_2 and NH_3 [113]. The aligned nanotubes produced were uniform and very straight and stood "individually" as shown in Figure 8d, in contrast to the aligned nanotubes produced by dense growth in which nanotubes were bundled together and wavy. The authors used a thin film Ni catalyst which was sputtered onto the glass substrates and also showed that plasma bombardment could be used to break up the thin film into islands. Furthermore, this work also demonstrated that the initial film thickness of the film could be used to control the diameter of the resultant nanotubes. Huang et al. later used this process to grow nanotubes uniformly on a polycrystalline Ni substrate which was pre-etched to create Ni islands [208]. Ren et al. [116] later used electron beam lithography to pattern submicrometer Ni dots directly on a silicon substrate and achieved the growth of single, freestanding vertical nanotubes. These nanotubes, however, were not very uniform in terms of height and yield which could be due to the absence of a diffusion barrier between the Ni catalyst and Si substrate. Huang et al. [264] next studied thin film Co, Fe, and Ni catalysts on a Ti substrate using the hot filament dc-PECVD process and found that the nanotubes produced with Ni were structurally the best in terms of graphitization, straightness, lack of amorphous carbon overcoating, and structural defects such as openings in the walls. The nanotubes nucleated from Ni also had the fastest growth rate (in terms of length). The authors noted that the diameters of the Ni catalyzed nanotubes were larger than the nanotubes catalyzed by Co and Fe, indicating that Ni had the weakest interaction with the Ti substrate and hence formed the largest catalytic clusters. Huang et al. studied the growth of individual nanotubes from patterned Ni dots and forests of nanotubes from a larger area Ni film [265]. They found that the Ni catalyst particle attained a particular orientation after growth, namely with the $\langle 220 \rangle$ orientated in the direction of the plasma. The individual nanotubes were also better crystallized with tubular walls, compared with the forests of nanotubes which had herringbone-like structures (i.e., nanofibers). They suggested that plasma focusing and heating of the catalyst particle in the case of the individual nanotube were responsible for its different structure.

Bower et al. devised an elegant set of experiments to investigate the alignment mechanism of the nanotubes [257]. A microwave PECVD system was used to grow carbon nanotubes catalyzed from a Co thin film on a Si substrate. Carbon nanotubes were deposited using PECVD and then the plasma was stopped for conventional thermal CVD to continue. The resultant nanotubes were thus straight for the plasma-grown section and curly for the thermally grown section. Additionally, when nonplanar or angled substrates were introduced into the plasma, the nanotubes still grew perpendicularly from the substrate surfaces because the microwave plasma formed a sheath around these objects. The authors concluded that the alignment was indeed a plasma induced effect and that it was probably the electric field in the plasma sheath formed around objects in the plasma which guided the growth of the nanotubes perpendicularly from the substrate. The electric field in the plasma sheath was estimated to be 0.1 V/μm, which is of the same order of magnitude as the electric field used to align single wall carbon nanotubes laterally during growth discussed previously.

Chen et al. [266], who used a hot filament dc-PECVD system, showed that by placing a substrate at an angle to the biased cathode, nanotubes also grew at an angle which followed the direction of the electric field in the plasma sheath. Tsai et al., who used a microwave plasma to synthesize aligned nanotubes, proposed a model based on anisotropic etching in order to explain the vertical alignment of the nanotubes [267]. They suggested that nanotubes which grew in random orientations were unprotected by their metal catalyst particle and were hence anisotropically etched away in the plasma [267].

Merkulov et al. developed a simple dc-PECVD system to grow vertically aligned carbon nanofibers [117]. The system used a resistively heated cathode which was biased at −550 V to generate a dc glow discharge. The gases used were C_2H_2 and NH_3, and Ni, deposited on top of a Ti

barrier layer on silicon substrates, was used as the catalyst. They investigated the lithographic conditions necessary to nucleate single, freestanding nanofibers as well as single-file lines of nanofibers. The maximum catalyst dimensions were determined to be 350 nm for a catalyst dot and 200 nm for the width of a catalyst line (i.e., for a single file line of nanofibers). Above these dimensions, the catalyst was observed to break into multiple nanoclusters at the growth temperature which nucleated more than one nanofiber. Merkulov et al. named their filaments nanofibers because they were highly disordered and bamboolike. In further studies, these authors found that the thickness of the catalyst layer controlled the average diameter of the nanofibers grown by PECVD [202], the ratio of C_2H_2 in the gas flow caused the nanofibers to attain a conical shape due to amorphous carbon buildup on walls of the nanofiber as it grew upward [268], and the direction of the nanofiber growth was determined by the local electric field in the plasma sheath [269]. The authors studied the field emission properties of their nanofibers and also fabricated gated microelectronic field emitters and electrochemical electrodes based on single nanofibers [54, 75, 270–272].

Chhowalla et al. performed a parametric study of the dc-PECVD growth of carbon nanotubes using C_2H_2 and NH_3 gases with Ni catalyst [182]. The structures were termed nanotubes because the filaments had well crystallized graphene walls parallel to the filament axis (see Fig. 3c for a typical TEM), with bamboo compartments along their axis. They studied the effect of the initial catalyst thickness (with thicker films leading to larger diameter nanotubes which were shorter and of lower density), the effect of the C_2H_2 ratio in the gas flow (with higher ratios leading to conical structures), the effect of pressure and deposition time (with higher pressures and longer times leading to longer nanotubes), and the effect of the dc bias on the substrate (with higher biases leading to straighter, aligned nanotubes). By examining the plasma characteristics, it was determined that 0.15 V/μm was the minimum electric field in the plasma sheath necessary for vertical alignment of the nanotubes. Clearly, to obtain a high degree of vertical alignment, one should thus maximize the electric field in the plasma sheath by increasing the substrate bias or by increasing the gas pressure (which increases ionization, leading to a higher field in the sheath). By investigating the effect of the growth temperature, it was found that the activation energy for PECVD growth was less (i.e., 0.76 eV) than that for thermal CVD (i.e., 1.21 eV), the latter being close to the bulk diffusion of carbon through Ni [204]. This indicates that the plasma plays a role in lowering the activation barrier necessary for nanotube growth. Teo et al. used the dc PECVD process to demonstrate the high yield and uniform growth of patterned areas of nanotubes and individual nanotubes [118, 273], examples of which are shown in Figure 5. In patterned growth especially, the C_2H_2 to NH_3 ratio was found to be important in achieving amorphous carbon free growth. During growth, the C_2H_2 is continuously being decomposed by the plasma (at a rate much faster than thermal pyrolysis) to form amorphous carbon on the substrate surface, and the role of NH_3 in the plasma is to etch away this unwanted amorphous carbon. The N and H species in the NH_3 plasma react with the amorphous carbon to form volatile C–N and C–H species. Hence, there exists an optimum condition, which was determined to be a flow ratio of 40:200 sccm of C_2H_2:NH_3 at 700 °C, where the production and etching of amorphous carbon is balanced, thus yielding substrates which are free of amorphous carbon. Teo et al. also found that individual vertical nanotubes, nucleated from Ni clusters of controlled size/volume, could be grown with a high degree of uniformity in terms of tip radius and height. The standard deviations in the tip diameter and height were found to be 4.1 and 6.3% of the average respectively [205]. This high degree of structural uniformity leads good uniformity in terms of field emission characteristics from adjacent nanotubes in an array [205, 274].

Delzeit et al. performed a parametric study of vertically aligned carbon nanotube and nanofiber growth in an inductively coupled plasma [149]. The authors used thin film Fe catalyst which was deposited on an aluminum layer on Si substrates, and the nanofibers/nanotubes were grown using CH_4, H_2, and Ar gases. By varying the process conditions, the authors found a clear transition between two structural forms of carbon filaments grown (i.e., the nanotube with parallel graphene walls and nanofiber with walls which were inclined to the filament axis). Until then, it was known that some plasma processes produced nanotubes (which were mostly bamboo), but other plasma processes produced nanofibers (with angled graphene layers but mostly hollow inside). The authors conclusively found that it was the relative amount of hydrogen species in the gas phase which determined whether nanotube or nanofiber growth was favored. Nanofiber growth was favored under process conditions which contained a large amount of hydrogen because the hydrogen could terminate the large number of dangling bonds protruding from angled graphene layers. The lack of hydrogen (e.g., achieved by Ar dilution) in the gas phase produced nanotubes which have closed, tubular graphene shells and few dangling bonds.

One of the most significant results recently is the demonstration of room temperature growth of nanofibers using rf-PECVD [242]. The authors used a CH_4 and H_2 plasma with Ni powder catalyst to grow nonaligned nanofibers at room temperature and at 100 and 250 °C. The authors claimed that instead of thermal energy, the energy of the plasma and induced rf heating of the catalyst particle allowed the formation of the carbon nanofibers at ambient temperature.

4.5. Growth of Branched Structures

The growth of branched filaments allows direct "wiring" of nanotube/nanofiber structures. Y-branched nanotubes would also allow switching and rectification behavior over a network of wires, similar to neural networks in biological systems. The growth of Y-branched nanotubes and nanofibers has been reported by several groups using the catalytic CVD [275–280]. Using the catalytic methods, the Y-junctions are generally formed at high temperatures (1000–1100 °C) [277, 279] or by using mixed or Cu catalysts [275, 276, 280–282]. For example, Chambers et al. found that branching is promoted when Co catalyst is alloyed with 2% Cu [275, 276] while Li et al. [280] observed branching when the catalyst is doped with Si or Ca. Another method for fabricating Y-junctions is to use a nanochannel alumina

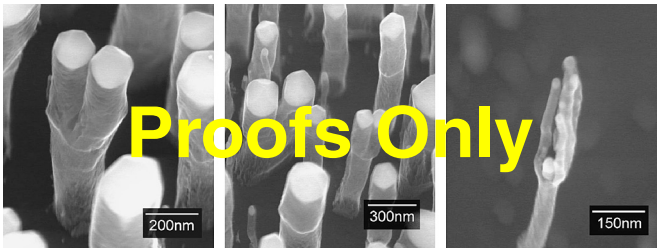

Figure 9. Branched structures as a result of a rapid drop in temperature from 700 to 550 °C during growth. The drop in temperature caused the Ni catalyst here (bright dot at the tip of the structure) to break up. After the temperature perturbation, the temperature was brought back to 700 °C for normal growth.

template that has been prepared such that the pores are Y-shaped [283, 284]. The electrical measurements on these Y-junction nanotubes showed nonlinear conductance and reproducible rectification [284].

It is also possible to grow branched structures without catalyst additives, templates, or high temperatures. In fact, all that is required is a simple perturbation during deposition in order to promote the formation of smaller catalyst particles (to catalyze branches) from a single, larger catalyst (which forms the main "stem"). In Figure 9, the branched nanofiber structures were formed by growth using dc-PECVD of C_2H_2:NH_3 with Ni catalyst at 700 °C for 3 minutes, then rapidly decreasing the growth temperature from 700 to 550 °C over ∼1 minute, and then normal deposition at 700 °C again for 3 minutes. As the solubility of carbon in the catalyst decreases at lower temperatures, the rapid drop in temperature causes the catalyst to become oversaturated and to split up to form more surface area to expel the carbon. After the catalyst has been broken up by the rapid drop in temperature, further growth at the normal temperature (700 °C) is used to extend the length of the nanofiber branches.

5. SUMMARY

Catalytic chemical vapor deposition is an extremely versatile technique for the production of carbon nanofibers and nanotubes. This chapter has shown that by controlling the catalyst and synthesis conditions, one can control many aspects of the growth, such as the structure (nanofiber vs nanotube), diameter, length, and alignment. The catalytic CVD technique can be adapted for mass production purposes or for the controlled growth of nanotubes/fibers at particular sites on a substrate for various applications.

GLOSSARY

Carbon nanofiber The carbon nanofiber is a generic term used to describe filaments/whiskers of carbon which have diameters less than 500 nm. The term fiber usually implies that the structures have a high aspect ratio, and hence the lengths of nanofibers are usually in the range of few micrometers or more. Although the carbon nanotube (see above) can be classed as a form of nanofiber, the carbon nanotube is typically used to describe structures which are comprised of tubular graphene walls parallel to the fiber axis. Recently, the term carbon nanofiber has been used for filaments which are comprised of graphene layers which are stacked at an angle to the fiber axis (such as the herringbone, cup-stacked, or stacked type filaments). Also, carbon nanofibers can be used to describe filaments of disordered/amorphous carbon.

Carbon nanotube The carbon nanotube is comprised of graphene sheets (containing hexagonally arranged, sp^2 bonded carbon atoms) which have been rolled up to form a seamless tubular structure. The simplest form is known as the single wall carbon nanotube in which the structure consists of a single graphene shell/tube. Multiwall carbon nanotubes consist of multiple, concentric tubular graphene shells.

ACKNOWLEDGMENTS

The authors thank M. Castignolles for the TEM image in Figure 3c, D. G. Hasko for use of electron beam lithography equipment to prepare Figure 5, and R. Lacerda for sample preparation. We also thank G. A. J. Amaratunga for invaluable discussions and help. K.B.K.T. acknowledges the support of Christ's College Cambridge. C.S. acknowledges the financial support of SIRIM Berhad (Malaysia), the Cambridge Commonwealth Trust, Selwyn College, and the Lundgren Fund.

REFERENCES

1. R. T. K. Baker, M. A. Barber, P. S. Harris, F. S. Feates, and R. J. Waite, *J. Catal.* 26, 51 (1972).
2. R. T. K. Baker, P. S. Harris, R. B. Thomas, and R. J. Waite, *J. Catal.* 30, 86 (1973).
3. R. T. K. Baker, *Carbon* 27, 315 (1989).
4. M. Endo, *Chemtech* 18, 568 (1988).
5. N. M. Rodriguez, A. Chambers, and R. T. K. Baker, *Langmuir* 11, 3862 (1995).
6. J. Gavillet, A. Loiseau, C. Journet, F. Willaime, F. Ducastelle, and J. C. Charlier, *Phys. Rev. Lett.* 8727, 275504 (2001).
7. C. A. Bessel, K. Laubernds, N. M. Rodriguez, and R. T. K. Baker, *J. Phys. Chem. B* 105, 1115 (2001).
8. M. Endo, Y. A. Kim, T. Hayashi, Y. Fukai, K. Oshida, M. Terrones, T. Yanagisawa, S. Higaki, and M. S. Dresselhaus, *Appl. Phys. Lett.* 80, 1267 (2002).
9. S. Iijima, *Nature* 354, 56 (1991).
10. http://www.fibrils.com, http://www.apsci.com/home.html, http://www.nanomirae.com/eng/main.htm, http://www.sdk.co.jp.
11. http://www.personal.rdg.ac.uk/∼scsharip/tubes.htm.
12. D. S. Bethune, C. H. Kiang, M. S. Devries, G. Gorman, R. Savoy, J. Vazquez, and R. Beyers, *Nature* 363, 605 (1993).
13. S. Iijima and T. Ichihashi, *Nature* 363, 603 (1993).
14. Y. Saito, T. Yoshikawa, S. Bandow, M. Tomita, and T. Hayashi, *Phys. Rev. B* 48, 1907 (1993).
15. M. Endo, K. Takeuchi, T. Hiraoka, T. Furuta, T. Kasai, X. Sun, C. H. Kiang, and M. S. Dresselhaus, *J. Phys. Chem. Solids* 58, 1707 (1997).
16. C. H. Kiang, M. Endo, P. M. Ajayan, G. Dresselhaus, and M. S. Dresselhaus, *Phys. Rev. Lett.* 81, 1869 (1998).
17. M. S. Dresselhaus and M. Endo, in "Carbon Nanotubes Synthesis, Structure, Properties and Applications" (M. S. Dresselhaus, G. Dresselhaus, and P. Avouris, Eds.), p. 11. Springer-Verlag, New York, 2001.

18. A. Bachtold, C. Strunk, J. P. Salvetat, J. M. Bonard, L. Forro, T. Nussbaumer, and C. Schonenberger, *Nature* 397, 673 (1999).
19. M. Endo, S. Iijima, and M. S. Dresselhaus, "Carbon Nanotubes." Elsevier Science, Oxford, 1996.
20. T. W. Odom, J. L. Huang, P. Kim, and C. M. Lieber, *Nature* 391, 62 (1998).
21. J. W. G. Wildoer, L. C. Venema, A. G. Rinzler, R. E. Smalley, and C. Dekker, *Nature* 391, 59 (1998).
22. L. Forro and C. Schnonenberger, in "Carbon Nanotubes Synthesis, Structure, Properties and Applications" (M. S. Dresselhaus, G. Dresselhaus, and P. Avouris, Eds.), p. 329. Springer-Verlag, New York, 2001.
23. R. Saito, G. Dresselhaus, and M. S. Dresselhaus, "Physical Properties of Carbon Nanotubes." Imperial College Press, London, 1998.
24. P. G. Collins and P. Avouris, *Sci. Am.* 283, 62 (2000).
25. E. W. Wong, P. E. Sheehan, and C. M. Lieber, *Science* 277, 1971 (1997).
26. M. F. Yu, O. Lourie, M. J. Dyer, K. Moloni, T. F. Kelly, and R. S. Ruoff, *Science* 287, 637 (2000).
27. M. F. Yu, B. S. Files, S. Arepalli, and R. S. Ruoff, *Phys. Rev. Lett.* 84, 5552 (2000).
28. J. Hone, M. Whitney, C. Piskoti, and A. Zettl, *Phys. Rev. B* 59, R2514 (1999).
29. P. Kim, L. Shi, A. Majumdar, and P. L. McEuen, *Phys. Rev. Lett.* 8721, 215502 (2001).
30. A. Thess, R. Lee, P. Nikolaev, H. J. Dai, P. Petit, J. Robert, C. H. Xu, Y. H. Lee, S. G. Kim, A. G. Rinzler, D. T. Colbert, G. E. Scuseria, D. Tomanek, J. E. Fischer, and R. E. Smalley, *Science* 273, 483 (1996).
31. C. Schonenberger, A. Bachtold, C. Strunk, J. P. Salvetat, and L. Forro, *Appl. Phys. A* 69, 283 (1999).
32. W. A. de Heer and R. Martel, *Phys. World* 13, 49 (2000).
33. S. Frank, P. Poncharal, Z. L. Wang, and W. A. de Heer, *Science* 280, 1744 (1998).
34. http://www.pa.msu.edu/cmp/csc/ntproperties/, compiled by T. A. Adams II.
35. R. H. Baughman, A. A. Zakhidov, and W. A. de Heer, *Science* 297, 787 (2002).
36. P. J. F. Harris, "Carbon Nanotubes and Related Structures. New Materials for the Twenty-first Century." Cambridge Univ. Press, Cambridge, UK, 1999.
37. T. W. Ebbesen, *Phys. Today* 49, 26 (1996).
38. H. J. Dai, *Surf. Sci.* 500, 218 (2002).
39. P. M. Ajayan, *Chem. Rev.* 99, 1787 (1999).
40. P. M. Ajayan and O. Z. Zhou, *Carbon Nanotubes Topics Appl. Phys.* 80, 391 (2001).
41. C. N. R. Rao, B. C. Satishkumar, A. Govindaraj, and M. Nath, *Chem. Phys. Chem.* 2, 78 (2001).
42. L. M. Dai and A. W. H. Mau, *Adv. Mater.* 13, 899 (2001).
43. W. B. Choi, D. S. Chung, J. H. Kang, H. Y. Kim, Y. W. Jin, I. T. Han, Y. H. Lee, J. E. Jung, N. S. Lee, G. S. Park, and J. M. Kim, *Appl. Phys. Lett.* 75, 3129 (1999).
44. A. G. Rinzler, J. H. Hafner, P. Nikolaev, L. Lou, S. G. Kim, D. Tomanek, P. Nordlander, D. T. Colbert, and R. E. Smalley, *Science* 269, 1550 (1995).
45. I. T. Han, H. J. Kim, Y. J. Park, N. Lee, J. E. Jang, J. W. Kim, J. E. Jung, and J. M. Kim, *Appl. Phys. Lett.* 81, 2070 (2002).
46. Y. H. Lee, Y. T. Jang, D. H. Kim, J. H. Ahn, and B. K. Ju, *Adv. Mater.* 13, 479 (2001).
47. D. S. Chung, S. H. Park, H. W. Lee, J. H. Choi, S. N. Cha, J. W. Kim, J. E. Jang, K. W. Min, S. H. Cho, M. J. Yoon, J. S. Lee, C. K. Lee, J. H. Yoo, J. M. Kim, J. E. Jung, Y. W. Jin, Y. J. Park, and J. B. You, *Appl. Phys. Lett.* 80, 4045 (2002).
48. W. B. Choi, Y. W. Jin, H. Y. Kim, S. J. Lee, M. J. Yun, J. H. Kang, Y. S. Choi, N. S. Park, N. S. Lee, and J. M. Kim, *Appl. Phys. Lett.* 78, 1547 (2001).
49. G. Z. Yue, Q. Qiu, B. Gao, Y. Cheng, J. Zhang, H. Shimoda, S. Chang, J. P. Lu, and O. Zhou, *Appl. Phys. Lett.* 81, 355 (2002).
50. N. deJonge, Y. Lanny, K. Schoots, and T. H. Ooesterkamp, *Nature* 420, 393 (2002).
51. R. Rosen, W. Simendinger, C. Debbault, H. Shimoda, L. Fleming, B. Stoner, and O. Zhou, *Appl. Phys. Lett.* 76, 1668 (2000).
52. http://www.oxfordxtg.com/products/coldcath.htm, Oxford Instruments plc., 2002.
53. C. J. Lee, T. J. Lee, and J. Park, *Chem. Phys. Lett.* 340, 413 (2001).
54. M. A. Guillorn, A. V. Melechko, V. I. Merkulov, E. D. Ellis, C. L. Britton, M. L. Simpson, D. H. Lowndes, and L. R. Baylor, *Appl. Phys. Lett.* 79, 3506 (2001).
55. H. J. Dai, J. H. Hafner, A. G. Rinzler, D. T. Colbert, and R. E. Smalley, *Nature* 384, 147 (1996).
56. H. Nishijima, S. Kamo, S. Akita, Y. Nakayama, K. I. Hohmura, S. H. Yoshimura, and K. Takeyasu, *Appl. Phys. Lett.* 74, 4061 (1999).
57. C. V. Nguyen, K. J. Chao, R. M. D. Stevens, L. Delzeit, A. Cassell, J. Han, and M. Meyyappan, *Nanotechnology* 12, 363 (2001).
58. http://www.piezomax.com, nPoint, 2002.
59. S. J. Tans, A. R. M. Verschueren, and C. Dekker, *Nature* 393, 49 (1998).
60. R. Martel, T. Schmidt, H. R. Shea, T. Hertel, and P. Avouris, *Appl. Phys. Lett.* 73, 2447 (1998).
61. V. Derycke, R. Martel, J. Appenzeller, and P. Avouris, *Nano Lett.* 1, 453 (2001).
62. A. Bachtold, P. Hadley, T. Nakanishi, and C. Dekker, *Science* 294, 1317 (2001).
63. J. Kong, N. R. Franklin, C. W. Zhou, M. G. Chapline, S. Peng, K. J. Cho, and H. J. Dai, *Science* 287, 622 (2000).
64. P. G. Collins, K. Bradley, M. Ishigami, and A. Zettl, *Science* 287, 1801 (2000).
65. K. Tsukagoshi, B. W. Alphenaar, and H. Ago, *Nature* 401, 572 (1999).
66. T. W. Tombler, C. W. Zhou, L. Alexseyev, J. Kong, H. J. Dai, L. Lei, C. S. Jayanthi, M. J. Tang, and S. Y. Wu, *Nature* 405, 769 (2000).
67. K. H. An, W. S. Kim, Y. S. Park, Y. C. Choi, S. M. Lee, D. C. Chung, D. J. Bae, S. C. Lim, and Y. H. Lee, *Adv. Mater.* 13, 497 (2001).
68. E. Frackowiak, K. Metenier, V. Bertagna, and F. Beguin, *Appl. Phys. Lett.* 77, 2421 (2000).
69. C. M. Niu, E. K. Sichel, R. Hoch, D. Moy, and H. Tennent, *Appl. Phys. Lett.* 70, 1480 (1997).
70. M. Hughes, M. S. P. Shaffer, A. C. Renouf, C. Singh, G. Z. Chen, J. Fray, and A. H. Windle, *Adv. Mater.* 14, 382 (2002).
71. M. Hughes, G. Z. Chen, M. S. P. Shaffer, D. J. Fray, and A. H. Windle, *Chem. Mater.* 14, 1610 (2002).
72. E. Frackowiak and F. Beguin, *Carbon* 40, 1775 (2002).
73. M. Endo, Y. A. Kim, T. Hayashi, K. Nishimura, T. Matusita, K. Miyashita, and M. S. Dresselhaus, *Carbon* 39, 1287 (2001).
74. J. Li, R. Stevens, L. Delzeit, H. T. Ng, A. Cassell, J. Han, and M. Meyyappan, *Appl. Phys. Lett.* 81, 910 (2002).
75. M. A. Guillorn, T. E. McKnight, A. Melechko, V. I. Merkulov, P. F. Britt, D. W. Austin, D. H. Lowndes, and M. L. Simpson, *J. Appl. Phys.* 91, 3824 (2002).
76. G. L. Che, B. B. Lakshmi, E. R. Fisher, and C. R. Martin, *Nature* 393, 346 (1998).
77. E. S. Steigerwalt, G. A. Deluga, D. E. Cliffel, and C. M. Lukehart, *J. Phys. Chem. B* 105, 8097 (2001).
78. A. Chambers, C. Park, R. T. K. Baker, and N. M. Rodriguez, *J. Phys. Chem. B* 102, 4253 (1998).
79. C. Park, P. E. Anderson, A. Chambers, C. D. Tan, R. Hidalgo, and N. M. Rodriguez, *J. Phys. Chem. B* 103, 10572 (1999).
80. A. C. Dillon, K. M. Jones, T. A. Bekkedahl, C. H. Kiang, D. S. Bethune, and M. J. Heben, *Nature* 386, 377 (1997).

81. B. Gao, A. Kleinhammes, X. P. Tang, C. Bower, L. Fleming, Y. Wu, and O. Zhou, *Chem. Phys. Lett.* 307, 153 (1999).
82. M. Hirscher, M. Becher, M. Haluska, U. Dettlaff-Weglikowska, A. Quintel, G. S. Duesberg, Y. M. Choi, P. Downes, M. Hulman, S. Roth, I. Stepanek, and P. Bernier, *Appl. Phys. A* 72, 129 (2001).
83. P. Kim and C. M. Lieber, *Science* 286, 2148 (1999).
84. R. H. Baughman, C. X. Cui, A. A. Zakhidov, Z. Iqbal, J. N. Barisci, G. M. Spinks, G. G. Wallace, A. Mazzoldi, D. De Rossi, A. G. Rinzler, O. Jaschinski, S. Roth, and M. Kertesz, *Science* 284, 1340 (1999).
85. J. Cumings and A. Zettl, *Science* 289, 602 (2000).
86. L. Zhang, A. V. Melechko, V. I. Merkulov, M. A. Guillorn, M. L. Simpson, D. H. Lowndes, and M. J. Doktycz, *Appl. Phys. Lett.* 81, 135 (2002).
87. J. Sandler, P. Werner, M. S. P. Shaffer, V. Demchuk, V. Altstadt, and A. H. Windle, *Compos. A* 33, 1033 (2002).
88. W. B. Downs and R. T. K. Baker, *J. Mater. Res.* 10, 625 (1995).
89. D. D. L. Chung, *Carbon* 39, 1119 (2001).
90. D. D. L. Chung, *Carbon* 39, 279 (2001).
91. J. Sandler, M. S. P. Shaffer, T. Prasse, W. Bauhofer, K. Schulte, and A. H. Windle, *Polymer* 40, 5967 (1999).
92. E. Kymakis and G. A. J. Amaratunga, *Appl. Phys. Lett.* 80, 112 (2002).
93. B. Vigolo, A. Penicaud, C. Coulon, C. Sauder, R. Pailler, C. Journet, P. Bernier, and P. Poulin, *Science* 290, 1331 (2000).
94. R. Andrews, D. Jacques, A. M. Rao, T. Rantell, F. Derbyshire, Y. Chen, J. Chen, and R. C. Haddon, *Appl. Phys. Lett.* 75, 1329 (1999).
95. P. A. O. Muisener, L. Clayton, J. D'Angelo, J. P. Harmon, A. K. Sikder, A. Kumar, A. M. Cassell, and M. Meyyappan, *J. Mater. Res.* 17, 2507 (2002).
96. P. Calvert, *Nature* 399, 210 (1999).
97. L. S. Schadler, S. C. Giannaris, and P. M. Ajayan, *Appl. Phys. Lett.* 73, 3842 (1998).
98. J. M. Bonard, N. Weiss, H. Kind, T. Stockli, L. Forro, K. Kern, and A. Chatelain, *Adv. Mater.* 13, 184 (2001).
99. L. Nilsson, O. Groening, C. Emmenegger, O. Kuettel, E. Schaller, L. Schlapbach, H. Kind, J. M. Bonard, and K. Kern, *Appl. Phys. Lett.* 76, 2071 (2000).
100. O. Groning, O. M. Kuttel, C. Emmenegger, P. Groning, and L. Schlapbach, *J. Vac. Sci. Technol. B* 18, 665 (2000).
101. T. W. Ebbesen and P. M. Ajayan, *Nature* 358, 220 (1992).
102. C. Journet, W. K. Maser, P. Bernier, A. Loiseau, M. L. delaChapelle, S. Lefrant, P. Deniard, R. Lee, and J. E. Fischer, *Nature* 388, 756 (1997).
103. "Chemistry and Physics of Carbon" (J. Philip, L. Walker, and P. A. Thrower, Eds.), Vol. 14. Dekker, New York/Basel, 1978.
104. R. T. K. Baker and P. S. Harris, in "Chemistry and Physics of Carbon" (J. P. L. Walker and P. A. Thrower, Eds.), Vol. 14, p. 83. Dekker, New York/Basel, 1978.
105. M. S. Dresselhaus, G. Dresselhaus, K. Sugihara, I. L. Spain, and H. A. Goldberg, "Graphite Fibers and Filaments," Vol. 5. Springer-Verlag, Berlin, 1988.
106. G. S. Duesberg, J. Muster, H. J. Byrne, S. Roth, and M. Burghard, *Appl. Phys. A* 69, 269 (1999).
107. A. G. Rinzler, J. Liu, H. Dai, P. Nikolaev, C. B. Huffman, F. J. Rodriguez-Macias, P. J. Boul, A. H. Lu, D. Heymann, D. T. Colbert, R. S. Lee, J. E. Fischer, A. M. Rao, P. C. Eklund, and R. E. Smalley, *Appl. Phys. A* 67, 29 (1998).
108. J. Kong, A. M. Cassell, and H. J. Dai, *Chem. Phys. Lett.* 292, 567 (1998).
109. J. H. Hafner, M. J. Bronikowski, B. R. Azamian, P. Nikolaev, A. G. Rinzler, D. T. Colbert, K. A. Smith, and R. E. Smalley, *Chem. Phys. Lett.* 296, 195 (1998).
110. S. S. Fan, M. G. Chapline, N. R. Franklin, T. W. Tombler, A. M. Cassell, and H. J. Dai, *Science* 283, 512 (1999).
111. Y. G. Zhang, A. L. Chang, J. Cao, Q. Wang, W. Kim, Y. M. Li, N. Morris, E. Yenilmez, J. Kong, and H. J. Dai, *Appl. Phys. Lett.* 79, 3155 (2001).
112. A. Ural, Y. Li, and H. Dai, *Appl. Phys. Lett.* 81, 3464 (2002).
113. Z. F. Ren, Z. P. Huang, J. W. Xu, J. H. Wang, P. Bush, M. P. Siegal, and P. N. Provencio, *Science* 282, 1105 (1998).
114. W. Z. Li, S. S. Xie, L. X. Qian, B. H. Chang, B. S. Zou, W. Y. Zhou, R. A. Zhao, and G. Wang, *Science* 274, 1701 (1996).
115. M. Terrones, N. Grobert, J. Olivares, J. P. Zhang, H. Terrones, K. Kordatos, W. K. Hsu, J. P. Hare, P. D. Townsend, K. Prassides, A. K. Cheetham, H. W. Kroto, and D. R. M. Walton, *Nature* 388, 52 (1997).
116. Z. F. Ren, Z. P. Huang, D. Z. Wang, J. G. Wen, J. W. Xu, J. H. Wang, L. E. Calvet, J. Chen, J. F. Klemic, and M. A. Reed, *Appl. Phys. Lett.* 75, 1086 (1999).
117. V. I. Merkulov, D. H. Lowndes, Y. Y. Wei, G. Eres, and E. Voelkl, *Appl. Phys. Lett.* 76, 3555 (2000).
118. K. B. K. Teo, M. Chhowalla, G. A. J. Amaratunga, W. I. Milne, D. G. Hasko, G. Pirio, P. Legagneux, F. Wyczisk, and D. Pribat, *Appl. Phys. Lett.* 79, 1534 (2001).
119. Z. W. Pan, S. S. Xie, B. H. Chang, C. Y. Wang, L. Lu, W. Liu, M. Y. Zhou, and W. Z. Li, *Nature* 394, 631 (1998).
120. L. An, J. M. Owens, L. E. McNeil, and J. Liu, *J. Am. Chem. Soc.* 124, 13688 (2002).
121. C. H. Choi, W. Kim, D. Wang, and H. Dai, *J. Phys. Chem. B*, in press.
122. H. J. Dai, J. Kong, C. W. Zhou, N. Franklin, T. Tombler, A. Cassell, S. S. Fan, and M. Chapline, *J. Phys. Chem. B* 103, 11246 (1999).
123. Y. C. Choi, Y. M. Shin, Y. H. Lee, B. S. Lee, G. S. Park, W. B. Choi, N. S. Lee, and J. M. Kim, *Appl. Phys. Lett.* 76, 2367 (2000).
124. N. M. Rodriguez, *J. Mater. Res.* 8, 3233 (1993).
125. H. G. Tennent, J. J. Barber, and R. Hoch, Hyperion Catalysis, Cambridge, MA, 1996.
126. S. B. Sinnott, R. Andrews, D. Qian, A. M. Rao, Z. Mao, E. C. Dickey, and F. Derbyshire, *Chem. Phys. Lett.* 315, 25 (1999).
127. G. G. Tibbetts, *Appl. Phys. Lett.* 42, 666 (1983).
128. A. Fonseca, K. Hernadi, P. Piedigrosso, J. F. Colomer, K. Mukhopadhyay, R. Doome, S. Lazarescu, L. P. Biro, P. Lambin, P. A. Thiry, D. Bernaerts, and J. B. Nagy, *Appl. Phys. A* 67, 11 (1998).
129. P. Piedigrosso, Z. Konya, J. F. Colomer, A. Fonseca, G. Van Tendeloo, and J. B. Nagy, *Phys. Chem. Chem. Phys.* 2, 163 (2000).
130. H. Q. Hou, A. K. Schaper, F. Weller, and A. Greiner, *Chem. Mater.* 14, 3990 (2002).
131. R. S. Wagner and W. C. Ellis, *Appl. Phys. Lett.* 4, 89 (1964).
132. R. S. Wagner, in "Whiskers Technology" (A. P. Levitt, Ed.), p. 47. Wiley, New York, 1970.
133. T. Baird, J. R. Fryer, and B. Grant, *Carbon* 12, 591 (1974).
134. A. Oberlin, M. Endo, and T. Koyama, *J. Crystal Growth* 32, 335 (1976).
135. A. Oberlin, M. Endo, and T. Koyama, *Carbon* 14, 133 (1976).
136. G. G. Tibbetts, *J. Crystal Growth* 66, 632 (1984).
137. H. J. Dai, A. G. Rinzler, P. Nikolaev, A. Thess, D. T. Colbert, and R. E. Smalley, *Chem. Phys. Lett.* 260, 471 (1996).
138. E. Boellaard, P. K. Debokx, A. Kock, and J. W. Geus, *J. Catal.* 96, 481 (1985).
139. P. K. Debokx, A. Kock, E. Boellaard, W. Klop, and J. W. Geus, *J. Catal.* 96, 454 (1985).
140. A. Kock, P. K. Debokx, E. Boellaard, W. Klop, and J. W. Geus, *J. Catal.* 96, 468 (1985).
141. E. Tracz, R. Scholz, and T. Borowiecki, *Appl. Catal.* 66, 133 (1990).
142. N. Krishnankutty, N. M. Rodriguez, and R. T. K. Baker, *J. Catal.* 158, 217 (1996).
143. A. Chambers and R. T. K. Baker, *J. Phys. Chem. B* 101, 1621 (1997).
144. M. S. Kim, N. M. Rodriguez, and R. T. K. Baker, *J. Catal.* 134, 253 (1992).

145. C. Park, E. S. Engel, A. Crowe, T. R. Gilbert, and N. M. Rodriguez, *Langmuir* 16, 8050 (2000).
146. C. Singh, T. Quested, C. B. Boothroyd, P. Thomas, I. A. Kinloch, A. I. Abou-Kandil, and A. H. Windle, *J. Phys. Chem. B* 106, 10915 (2002).
147. H. Terrones, T. Hayashi, M. Munoz-Navia, M. Terrones, Y. A. Kim, N. Grobert, R. Kamalakaran, J. Dorantes-Davila, R. Escudero, M. S. Dresselhaus, and M. Endo, *Chem. Phys. Lett.* 343, 241 (2001).
148. P. E. Nolan, D. C. Lynch, and A. H. Cutler, *J. Phys. Chem. B* 102, 4165 (1998).
149. L. Delzeit, I. McAninch, B. A. Cruden, D. Hash, B. Chen, J. Han, and M. Meyyappan, *J. Appl. Phys.* 91, 6027 (2002).
150. H. W. Kroto, J. R. Heath, S. C. Obrien, R. F. Curl, and R. E. Smalley, *Nature* 318, 162 (1985).
151. J. Kong, H. T. Soh, A. M. Cassell, C. F. Quate, and H. J. Dai, *Nature* 395, 878 (1998).
152. A. M. Cassell, J. A. Raymakers, J. Kong, and H. J. Dai, *J. Phys. Chem. B* 103, 6484 (1999).
153. M. Su, B. Zheng, and J. Liu, *Chem. Phys. Lett.* 322, 321 (2000).
154. B. Kitiyanan, W. E. Alvarez, J. H. Harwell, and D. E. Resasco, *Chem. Phys. Lett.* 317, 497 (2000).
155. W. E. Alvarez, B. Kitiyanan, A. Borgna, and D. E. Resasco, *Carbon* 39, 547 (2001).
156. J. E. Herrera, L. Balzano, A. Borgna, W. E. Alvarez, and D. E. Resasco, *J. Catal.* 204, 129 (2001).
157. W. E. Alvarez, F. Pompeo, J. E. Herrera, L. Balzano, and D. E. Resasco, *Chem. Mater.* 14, 1853 (2002).
158. A. Kukovecz, Z. Konya, N. Nagaraju, I. Willems, A. Tamasi, A. Fonseca, J. B. Nagy, and I. Kiricsi, *Phys. Chem. Chem. Phys.* 2, 3071 (2000).
159. Y. M. Li, W. Kim, Y. G. Zhang, M. Rolandi, D. W. Wang, and H. J. Dai, *J. Phys. Chem. B* 105, 11424 (2001).
160. C. L. Cheung, A. Kurtz, H. Park, and C. M. Lieber, *J. Phys. Chem. B* 106, 2429 (2002).
161. J. F. Colomer, G. Bister, I. Willems, Z. Konya, A. Fonseca, G. Van Tendeloo, and J. B. Nagy, *Chem. Commun.* 1343 (1999).
162. J. Geng, C. Singh, D. Shephard, M. Shaffer, B. F. G. Johnson, and A. H. Windle, *Chem. Commun.* 2666 (2002).
163. V. Ivanov, J. B. Nagy, P. Lambin, A. Lucas, X. B. Zhang, X. F. Zhang, D. Bernaerts, G. Vantendeloo, S. Amelinckx, and J. Vanlanduyt, *Chem. Phys. Lett.* 223, 329 (1994).
164. L. F. Sun, J. M. Mao, Z. W. Pan, B. H. Chang, W. Y. Zhou, G. Wang, L. X. Qian, and S. S. Xie, *Appl. Phys. Lett.* 74, 644 (1999).
165. H. J. Dai, *Phys. World* 13, 43 (2000).
166. S. Amelinckx, X. B. Zhang, D. Bernaerts, X. F. Zhang, V. Ivanov, and J. B. Nagy, *Science* 265, 635 (1994).
167. C. J. Lee and J. Park, *Appl. Phys. Lett.* 77, 3397 (2000).
168. W. Z. Li, J. G. Wen, Y. Tu, and Z. F. Ren, *Appl. Phys. A* 73, 259 (2001).
169. Y. Li, J. Liu, Y. Q. Wang, and Z. L. Wang, *Chem. Mater.* 13, 1008 (2001).
170. H. Ago, S. Ohshima, K. Uchida, and M. Yumura, *J. Phys. Chem. B* 105, 10453 (2001).
171. L. Delzeit, B. Chen, A. Cassell, R. Stevens, C. Nguyen, and M. Meyyappan, *Chem. Phys. Lett.* 348, 368 (2001).
172. P. Nikolaev, M. J. Bronikowski, R. K. Bradley, F. Rohmund, D. T. Colbert, K. A. Smith, and R. E. Smalley, *Chem. Phys. Lett.* 313, 91 (1999).
173. M. Joseyacaman, M. Mikiyoshida, L. Rendon, and J. G. Santiesteban, *Appl. Phys. Lett.* 62, 657 (1993).
174. M. Endo, K. Takeuchi, S. Igarashi, K. Kobori, M. Shiraishi, and H. W. Kroto, *J. Phys. Chem. Solids* 54, 1841 (1993).
175. A. M. Benito, Y. Maniette, E. Munoz, and M. T. Martinez, *Carbon* 36, 681 (1998).
176. N. R. Franklin, Y. M. Li, R. J. Chen, A. Javey, and H. J. Dai, *Appl. Phys. Lett.* 79, 4571 (2001).
177. N. R. Franklin and H. J. Dai, *Adv. Mater.* 12, 890 (2000).
178. V. I. Merkulov, A. V. Melechko, M. A. Guillorn, D. H. Lowndes, and M. L. Simpson, *Chem. Phys. Lett.* 350, 381 (2001).
179. D. S. Y. Hsu, *Appl. Phys. Lett.* 80, 2988 (2002).
180. C. Bower, W. Zhu, D. Shalom, D. Lopez, L. H. Chen, P. L. Gammel, and S. Jin, *Appl. Phys. Lett.* 80, 3820 (2002).
181. G. Pirio, P. Legagneux, D. Pribat, K. B. K. Teo, M. Chhowalla, G. A. J. Amaratunga, and W. I. Milne, *Nanotechnology* 13, 1 (2002).
182. M. Chhowalla, K. B. K. Teo, C. Ducati, N. L. Rupesinghe, G. A. J. Amaratunga, A. C. Ferrari, D. Roy, J. Robertson, and W. I. Milne, *J. Appl. Phys.* 90, 5308 (2001).
183. C. Bower, O. Zhou, W. Zhu, D. J. Werder, and S. H. Jin, *Appl. Phys. Lett.* 77, 2767 (2000).
184. J. I. Sohn, S. Lee, Y. H. Song, S. Y. Choi, K. I. Cho, and K. S. Nam, *Appl. Phys. Lett.* 78, 901 (2001).
185. S. M. Sze, "VLSI Technology," 2nd ed., p. 309. McGraw-Hill, New York, 1988.
186. K. B. K. Teo, M. Chhowalla, G. A. J. Amaratunga, W. I. Milne, G. Pirio, P. Legagneux, F. Wyczisk, D. Pribat, and D. G. Hasko, *Appl. Phys. Lett.* 80, 2011 (2002).
187. A. M. Rao, D. Jacques, R. C. Haddon, W. Zhu, C. Bower, and S. Jin, *Appl. Phys. Lett.* 76, 3813 (2000).
188. T. de los Arcos, F. Vonau, M. G. Garnier, V. Thommen, H. G. Boyen, P. Oelhafen, M. Duggelin, D. Mathis, and R. Guggenheim, *Appl. Phys. Lett.* 80, 2383 (2002).
189. U. Gonser, A. Mooradian, K. A. Muller, M. B. Panish, and H. Sakaki, in "Graphite Fibers and Filaments" (M. S. Dresselhaus, G. Dresselhaus, K. Sugihara, I. L. Spain, and H. A. Goldberg, Eds.), Vol. 5, p. 382. Springer-Verlag, Berlin, 1988.
190. C. Emmenegger, P. Mauron, A. Zuttel, C. Nutzenadel, A. Schneuwly, R. Gallay, and L. Schlapbach, *Appl. Surf. Sci.* 162, 452 (2000).
191. H. Kind, J. M. Bonard, C. Emmenegger, L. O. Nilsson, K. Hernadi, E. Maillard-Schaller, L. Schlapbach, L. Forro, and K. Kern, *Adv. Mater.* 11, 1285 (1999).
192. R. T. K. Baker, J. R. Alonzo, J. A. Dumesic, and D. J. C. Yates, *J. Catal.* 77, 74 (1982).
193. S. K. Hwang, K. D. Lee, and K. H. Lee, *Jpn. J. Appl. Phys. 2 Lett.* 40, L580 (2001).
194. A. M. Cassell, S. Verma, L. Delzeit, M. Meyyappan, and J. Han, *Langmuir* 17, 260 (2001).
195. B. Chen, G. Parker, J. Han, M. Meyyappan, and A. M. Cassell, *Chem. Mater.* 14, 1891 (2002).
196. Y. Tu, Z. P. Huang, D. Z. Wang, J. G. Wen, and Z. F. Ren, *Appl. Phys. Lett.* 80, 4018 (2002).
197. J. F. Colomer, C. Stephan, S. Lefrant, G. Van Tendeloo, I. Willems, Z. Konya, A. Fonseca, C. Laurent, and J. B. Nagy, *Chem. Phys. Lett.* 317, 83 (2000).
198. J. M. Bonard, T. Stockli, O. Noury, and A. Chatelain, *Appl. Phys. Lett.* 78, 2775 (2001).
199. K. Matsumoto, S. Kinosita, Y. Gotoh, T. Uchiyama, S. Manalis, and C. Quate, *Appl. Phys. Lett.* 78, 539 (2001).
200. J. H. Hafner, C. L. Cheung, and C. M. Lieber, *Nature* 398, 761 (1999).
201. E. B. Cooper, S. R. Manalis, H. Fang, H. Dai, K. Matsumoto, S. C. Minne, T. Hunt, and C. F. Quate, *Appl. Phys. Lett.* 75, 3566 (1999).
202. Y. Y. Wei, G. Eres, V. I. Merkulov, and D. H. Lowndes, *Appl. Phys. Lett.* 78, 1394 (2001).
203. M. P. Siegal, D. L. Overmyer, and P. P. Provencio, *Appl. Phys. Lett.* 80, 2171 (2002).
204. C. Ducati, I. Alexandrou, M. Chhowalla, G. A. J. Amaratunga, and J. Robertson, *J. Appl. Phys.* 92, 3299 (2002).
205. K. B. K. Teo, S. B. Lee, M. Chhowalla, D. G. Hasko, H. Ahmed, G. A. J. Amaratunga, W. I. Milne, V. Semet, V. T. Binh, O. Groening, M. Castignolles, A. Loiseau, P. Legagneux, G. Pirio, and D. Pribat, *Nanotechnology*, in press.

206. Y. Chen, Z. L. Wang, J. S. Yin, D. J. Johnson, and R. H. Prince, *Chem. Phys. Lett.* 272, 178 (1997).
207. Y. Chen, S. Patel, Y. G. Ye, S. T. Shaw, and L. P. Luo, *Appl. Phys. Lett.* 73, 2119 (1998).
208. Z. P. Huang, J. W. Wu, Z. F. Ren, J. H. Wang, M. P. Siegal, and P. N. Provencio, *Appl. Phys. Lett.* 73, 3845 (1998).
209. T. Sato, D. G. Hasko, and H. Ahmed, *J. Vac. Sci. Technol. B* 15, 45 (1997).
210. T. Koyama, *Carbon* 10, 757 (1972).
211. T. Kato, K. Kusakabe, and S. Morooka, *J. Mater. Sci. Lett.* 11, 674 (1992).
212. L. J. Ci, Y. H. Li, B. Q. Wei, J. Liang, C. L. Xu, and D. H. Wu, *Carbon* 38, 1933 (2000).
213. M. Endo, K. Takeuchi, K. Kobori, K. Takahashi, H. W. Kroto, and A. Sarkar, *Carbon* 33, 873 (1995).
214. B. C. Satishkumar, A. Govindaraj, and C. N. R. Rao, *Chem. Phys. Lett.* 307, 158 (1999).
215. R. Sen, A. Govindaraj, and C. N. R. Rao, *Chem. Phys. Lett.* 267, 276 (1997).
216. S. M. Huang, L. M. Dai, and A. W. H. Mau, *J. Phys. Chem. B* 103, 4223 (1999).
217. Y. Y. Yang, S. M. Huang, H. Z. He, A. W. H. Mau, and L. M. Dai, *J. Am. Chem. Soc.* 121, 10832 (1999).
218. D. C. Li, L. M. Dai, S. M. Huang, A. W. H. Mau, and Z. L. Wang, *Chem. Phys. Lett.* 316, 349 (2000).
219. C. Singh, M. S. P. Shaffer, and A. H. Windle, *Carbon* 41, 363 (2003).
220. R. Sen, A. Govindaraj, and C. N. R. Rao, *Chem. Mater.* 9, 2078 (1997).
221. R. Andrews, D. Jacques, A. M. Rao, F. Derbyshire, D. Qian, X. Fan, E. C. Dickey, and J. Chen, *Chem. Phys. Lett.* 303, 467 (1999).
222. R. Kamalakaran, M. Terrones, T. Seeger, P. Kohler-Redlich, M. Ruhle, Y. A. Kim, T. Hayashi, and M. Endo, *Appl. Phys. Lett.* 77, 3385 (2000).
223. M. Mayne, N. Grobert, M. Terrones, R. Kamalakaran, M. Ruhle, H. W. Kroto, and D. R. M. Walton, *Chem. Phys. Lett.* 338, 101 (2001).
224. Z. J. Zhang, B. Q. Wei, G. Ramanath, and P. M. Ajayan, *Appl. Phys. Lett.* 77, 3764 (2000).
225. B. Q. Wei, R. Vajtai, Y. Jung, J. Ward, R. Zhang, G. Ramanath, and P. M. Ajayan, *Nature* 416, 495 (2002).
226. B. Q. Wei, Z. J. Zhang, G. Ramanath, and P. M. Ajayan, *Appl. Phys. Lett.* 77, 2985 (2000).
227. A. Y. Cao, L. J. Ci, D. J. Li, B. Q. Wei, C. L. Xu, J. Liang, and D. H. Wu, *Chem. Phys. Lett.* 335, 150 (2001).
228. R. Vajtai, K. Kordas, B. Q. Wei, J. Bekesi, S. Leppavuori, T. F. George, and P. M. Ajayan, *Mater. Sci. Eng. C* 19, 271 (2002).
229. B. Q. Wei, R. Vajtai, Z. J. Zhang, G. Ramanath, and P. M. Ajayan, *J. Nanosci. Nanotechnol.* 1, 35 (2001).
230. C. N. R. Rao, A. Govindaraj, R. Sen, and B. C. Satishkumar, *Mater. Res. Innov.* 2, 128 (1998).
231. H. M. Cheng, F. Li, G. Su, H. Y. Pan, L. L. He, X. Sun, and M. S. Dresselhaus, *Appl. Phys. Lett.* 72, 3282 (1998).
232. H. W. Zhu, C. L. Xu, D. H. Wu, B. Q. Wei, R. Vajtai, and P. M. Ajayan, *Science* 296, 884 (2002).
233. H. W. Zhu, B. Jiang, C. L. Xu, and D. H. Wu, *Chem. Commun.* 1858 (2002).
234. B. Q. Wei, R. Vajtai, Y. Y. Choi, P. M. Ajayan, H. W. Zhu, C. L. Xu, and D. H. Wu, *Nano Lett.* 2, 1105 (2002).
235. M. J. Bronikowski, P. A. Willis, D. T. Colbert, K. A. Smith, and R. E. Smalley, *J. Vac. Sci. Technol. A* 19, 1800 (2001).
236. HSC Chemistry Version 4.1, Outokumpu Research Oy, 2002.
237. "Chemistry and Physics of Carbon" (J. Philip, L. Walker, and P. A. Thrower, Eds.), Vol. 7. Dekker, New York, 1971.
238. V. Ivanov, A. Fonseca, J. B. Nagy, A. Lucas, P. Lambin, D. Bernaerts, and X. B. Zhang, *Carbon* 33, 1727 (1995).
239. J.-B. Donnet and R. C. Bansal, "Carbon Fibers," 2nd ed., Vol. 10. Dekker, New York, 1990.
240. C. Singh, M. S. P. Shaffer, I. Kinloch, and A. H. Windle, *Physica B* 323, 339 (2002).
241. J. M. Bonard, M. Croci, F. Conus, T. Stockli, and A. Chatelain, *Appl. Phys. Lett.* 81, 2836 (2002).
242. B. O. Boskovic, V. Stolojan, R. U. A. Khan, S. Haq, and S. R. P. Silva, *Nature Mater.* 27 Oct 2002 (online publication).
243. S. Ohshima, H. Ago, H. Inoue, and M. Yumura, *New Diam. Front. Carbon Technol.* 11, 437 (2001).
244. Y. Wang, F. Wei, G. Luo, H. Yu, and G. Gu, *Chem. Phys. Lett.* 364, 568 (2002).
245. Y. Wang, F. Wei, G. Gu, and H. Yu, *Physica B* 322, 327 (2002).
246. A. Weidenkaff, S. G. Ebbinghaus, P. Mauron, A. Reller, Y. Zhang, and A. Zuttel, *Mater. Sci. Eng. C* 19, 119 (2002).
247. A. Huczko, *Appl. Phys. A* 70, 365 (2000).
248. T. Kyotani, L. F. Tsai, and A. Tomita, *Chem. Mater.* 7, 1427 (1995).
249. G. Che, B. B. Lakshmi, C. R. Martin, E. R. Fisher, and R. S. Ruoff, *Chem. Mater.* 10, 260 (1998).
250. J. Li, C. Papadopoulos, J. M. Xu, and M. Moskovits, *Appl. Phys. Lett.* 75, 367 (1999).
251. N. Wang, Z. K. Tang, G. D. Li, and J. S. Chen, *Nature* 408, 50 (2000).
252. Y. Avigal and R. Kalish, *Appl. Phys. Lett.* 78, 2291 (2001).
253. H. T. Soh, C. F. Quate, A. F. Morpurgo, C. M. Marcus, J. Kong, and H. J. Dai, *Appl. Phys. Lett.* 75, 627 (1999).
254. J. Kong, C. Zhou, A. Morpurgo, H. T. Soh, C. F. Quate, C. Marcus, and H. Dai, *Appl. Phys. A* 69, 305 (1999).
255. Y. H. Lee, Y. T. Jang, C. H. Choi, D. H. Kim, C. W. Lee, J. E. Lee, Y. S. Han, S. S. Yoon, J. K. Shin, S. T. Kim, E. K. Kim, and B. K. Ju, *Adv. Mater.* 13, 1371 (2001).
256. H. Conrads and M. Schmidt, *Plasma Sources Sci. Technol.* 9, 441 (2000).
257. C. Bower, W. Zhu, S. H. Jin, and O. Zhou, *Appl. Phys. Lett.* 77, 830 (2000).
258. L. C. Qin, D. Zhou, A. R. Krauss, and D. M. Gruen, *Appl. Phys. Lett.* 72, 3437 (1998).
259. N. Wang and B. D. Yao, *Appl. Phys. Lett.* 78, 4028 (2001).
260. M. Okai, T. Muneyoshi, T. Yaguchi, and S. Sasaki, *Appl. Phys. Lett.* 77, 3468 (2000).
261. Y. C. Choi, Y. M. Shin, S. C. Lim, D. J. Bae, Y. H. Lee, B. S. Lee, and D. C. Chung, *J. Appl. Phys.* 88, 4898 (2000).
262. H. Murakami, M. Hirakawa, C. Tanaka, and H. Yamakawa, *Appl. Phys. Lett.* 76, 1776 (2000).
263. K.-Y. Lee, K. Fujimoto, S. Ohkura, S. Honda, M. Katayama, T. Hirao, and K. Oura, *Mater. Res. Soc. Symp. Proc.* 675, W3.1 (2001).
264. Z. P. Huang, D. Z. Wang, J. G. Wen, M. Sennett, H. Gibson, and Z. F. Ren, *Appl. Phys. A* 74, 387 (2002).
265. J. G. Wen, Z. P. Huang, D. Z. Wang, J. H. Chen, S. X. Yang, Z. F. Ren, J. H. Wang, L. E. Calvet, J. Chen, J. F. Klemic, and M. A. Reed, *J. Mater. Res.* 16, 3246 (2001).
266. Y. Chen, D. T. Shaw, and L. P. Guo, *Appl. Phys. Lett.* 76, 2469 (2000).
267. S. H. Tsai, C. W. Chao, C. L. Lee, and H. C. Shih, *Appl. Phys. Lett.* 74, 3462 (1999).
268. V. I. Merkulov, M. A. Guillorn, D. H. Lowndes, M. L. Simpson, and E. Voelkl, *Appl. Phys. Lett.* 79, 1178 (2001).
269. V. I. Merkulov, A. V. Melechko, M. A. Guillorn, M. L. Simpson, D. H. Lowndes, J. H. Whealton, and R. J. Raridon, *Appl. Phys. Lett.* 80, 4816 (2002).
270. L. R. Baylor, V. I. Merkulov, E. D. Ellis, M. A. Guillorn, D. H. Lowndes, A. V. Melechko, M. L. Simpson, and J. H. Whealton, *J. Appl. Phys.* 91, 4602 (2002).
271. M. A. Guillorn, M. D. Hale, V. I. Merkulov, M. L. Simpson, G. Y. Eres, H. Cui, A. A. Puretzky, and D. B. Geohegan, *Appl. Phys. Lett.* 81, 2860 (2002).

272. V. I. Merkulov, D. H. Lowndes, and L. R. Baylor, *J. Appl. Phys.* 89, 1933 (2001).
273. K. B. K. Teo, M. Chhowalla, G. A. J. Amaratunga, W. I. Milne, G. Pirio, P. Legagneux, F. Wyczisk, J. Olivier, and D. Pribat, *J. Vac. Sci. Technol. B* 20, 116 (2002).
274. V. Semet, V. T. Binh, P. Vincent, D. Guillot, K. B. K. Teo, M. Chhowalla, G. A. J. Amaratunga, W. I. Milne, P. Legagneux, and D. Pribat, *Appl. Phys. Lett.* 81, 343 (2002).
275. A. Chambers, N. M. Rodriguez, and R. T. K. Baker, *J. Phys. Chem.* 99, 10581 (1995).
276. A. Chambers, N. M. Rodriguez, and R. T. K. Baker, *J. Mater. Res.* 11, 430 (1996).
277. B. C. Satishkumar, P. J. Thomas, A. Govindaraj, and C. N. R. Rao, *Appl. Phys. Lett.* 77, 2530 (2000).
278. F. L. Deepak, A. Govindaraj, and C. N. R. Rao, *Chem. Phys. Lett.* 345, 5 (2001).
279. J. M. Ting and C. C. Chang, *Appl. Phys. Lett.* 80, 324 (2002).
280. W. Z. Li, J. G. Wen, and Z. F. Ren, *Appl. Phys. Lett.* 79, 1879 (2001).
281. B. Gan, J. Ahn, Q. Zhang, S. F. Yoon, Rusli, Q. F. Huang, H. Yang, M. B. Yu, and W. Z. Li, *Diam. Relat. Mater.* 9, 897 (2000).
282. B. Gan, J. Ahn, Q. Zhang, Rusli, S. F. Yoon, J. Yu, Q. F. Huang, K. Chew, V. A. Ligatchev, X. B. Zhang, and W. Z. Li, *Chem. Phys. Lett.* 333, 23 (2001).
283. J. Li, C. Papadopoulos, and J. Xu, *Nature* 402, 253 (1999).
284. C. Papadopoulos, A. Rakitin, J. Li, A. S. Vedeneev, and J. M. Xu, *Phys. Rev. Lett.* 85, 3476 (2000).